

# Aneuploidy can be an evolutionary diversion on the path to adaptation

Ilia Kohanovski<sup>a,b,1</sup>, Martin Pontz<sup>a,1</sup>, Pétra Vande Zande<sup>c</sup>, Anna Selmecki<sup>c</sup>, Orna  
Dahan<sup>d</sup>, Yitzhak Pilpel<sup>d</sup>, Avihu H. Yona<sup>e</sup>, and Yoav Ram<sup>a,\*</sup>

<sup>a</sup>School of Zoology, Faculty of Life Sciences, Tel Aviv University, Tel Aviv, Israel

<sup>b</sup>School of Computer Science, Reichman University, Herzliya, Israel

<sup>c</sup>Department of Microbiology and Immunology, University of Minnesota Medical School, Minneapolis, MN

<sup>d</sup>Department of Molecular Genetics, Weizmann Institute of Science, Rehovot, Israel

<sup>e</sup>Institute of Biochemistry, Food Science and Nutrition, Robert H. Smith Faculty of Agriculture, Food and  
Environment, The Hebrew University of Jerusalem, Israel

<sup>1</sup>These authors contributed equally to this work

\*Corresponding author: yoav@yoavram.com

January 21, 2024

Classifications. Biological Sciences: Evolution, Genetics, Microbiology, Population Biology.

Keywords: whole-chromosome duplication, evolutionary model, adaptive evolution

**Abstract**

Aneuploidy is common in eukaryotes, often leading to decreased fitness. However, evidence from fungi and human tumour cells suggests that specific aneuploidies can be beneficial under stressful conditions and facilitate adaptation. In a previous evolutionary experiment with yeast, populations evolving under heat stress became aneuploid, only to later revert to euploidy after beneficial mutations accumulated. It was therefore suggested that aneuploidy is a "stepping stone" on the path to adaptation. Here, we test this hypothesis. We use Bayesian inference to fit an evolutionary model with both aneuploidy and mutation the experimental results. We then predict the genotype frequency dynamics during the experiment, demonstrating that most of the evolved euploid population likely did not descend from aneuploid cells, but rather from the euploid wildtype population. Our model shows how the beneficial mutation supply—the product of population size and beneficial mutation rate—determines the evolutionary dynamics: with low supply, much of the evolved population descends from aneuploid cells; but with high supply, beneficial mutations are generated fast enough to outcompete aneuploidy due to its inherent fitness cost. Our results suggest that despite its potential fitness benefits under stress, aneuploidy can be an evolutionary "diversion" rather than a "stepping stone": it can delay, rather than facilitate, the adaptation of the population, and cells that become aneuploid may leave less descendants compared to cells that remain diploid.

## 34 Introduction

Aneuploidy is an imbalance in the number of chromosomes in the cell: an incorrect karyotype.  
36 Evidence suggests aneuploidy is very common in eukaryotes, e.g. animals<sup>49,38,2</sup>, and fungi<sup>41,73,45,62</sup>.  
Aneuploidy has been implicated in cancer formation, progression, and drug resistance<sup>4,51,49,48,23,34</sup>.  
38 It is also common in protozoan pathogens of the *Leishmania* genus, a major global health concern<sup>36</sup>,  
and contributes to the emergence of drug resistance<sup>52</sup> and virulence<sup>37</sup> in fungal pathogens, which  
40 are under-studied<sup>47</sup>, despite infecting a billion people per year, causing significant morbidity in >150  
million and death in >1.5 million people per year<sup>52,47</sup>.  
42 Experiments with human and mouse embryos found that most germ-line aneuploidies are lethal. Ane-  
uploidies are also associated with developmental defects and lethality in other multicellular organ-  
44 isms<sup>55</sup>. For example, aneuploid mouse embryonic cells grow slower than euploid cells<sup>67</sup>. Similarly,  
in unicellular eukaryotes growing in benign conditions, aneuploidy usually leads to slower growth and  
46 decreased overall fitness, in part due to proteotoxic stress due to increased expression, gene dosage  
imbalance, and hypo-osmotic-like stress<sup>39,65,41,55,50,27,72,66,68,46</sup>.  
48 However, aneuploidy can be beneficial under stressful conditions due to the wide range of phenotypes  
it can produce, some of which are advantageous<sup>41,68</sup>. Indeed, in a survey of 1,011 yeast strains,  
50 aneuploidy has been detected in about 19%<sup>42</sup>. Thus, aneuploidy can lead to rapid adaptation in  
unicellular eukaryotes<sup>17,64,21,44</sup>, as well as to rapid growth of somatic tumour cells<sup>51,57</sup>. For example,  
52 aneuploidy in *Saccharomyces cerevisiae* facilitates adaptation to a variety of stressful conditions like  
heat and pH<sup>70</sup>, copper<sup>8,17</sup>, salt<sup>11,46</sup>, and nutrient limitation<sup>12,19,1</sup>, with similar results in *Candida*  
54 *albicans*<sup>68</sup>. Importantly, aneuploidy can also lead to drug resistance in pathogenic fungi such as  
*C. albicans*<sup>54,53,16</sup> and *Cryptococcus neoformans*<sup>58</sup>, which cause candidiasis and meningoencephalitis,  
56 respectively. Although we focus here on aneuploidy, a similar phenomena of adaptation via gene  
duplication or amplification has been observed in yeast<sup>33</sup>, bacteria<sup>60</sup>, and DNA viruses<sup>13</sup>.  
58 Yona et al.<sup>70</sup> demonstrated experimentally the importance of aneuploidy in adaptive evolution. They  
evolved populations of *S. cerevisiae* under strong heat stress. The populations adapted to the heat stress  
60 within 450 generations, and this adaptation was determined to be due a duplication of Chromosome  
III. Later on, after more than 1,500 generations, the populations reverted back to an euploid state, while  
62 remaining adapted to the heat stress. Aneuploidy was therefore suggested to be a *transient adaptive*  
*solution*, because it can rapidly appear and fixate in the population under stressful conditions, and can  
64 then be rapidly lost when the cost of aneuploidy outweighs its benefit—after the stress is removed,  
or after "refined" beneficial mutations appear and fixate<sup>70</sup>. Furthermore, it has been suggested that

66 aneuploidy is an evolutionary "stepping stone" that facilitates future adaptation by genetic mutations,  
which require more time to evolve<sup>70,69</sup>.

68 Here, we test the hypothesis that aneuploidy is a an *evolutionary stepping stone* that facilitates adaptive  
evolution by genetic mutations Yona et al.<sup>69</sup>. We develop an evolutionary genetic model and fit it to the  
70 experimental results of Yona et al.<sup>70</sup> to predict the genotype frequency dynamics in the experimental  
populations, thereby estimating the frequency of evolved euploid cells that descended from aneuploid  
72 cells. Our results show that although aneuploidy reached high frequencies in the experimental  
populations, the majority of cells in the evolved euploid population likely did not descend from  
74 aneuploid cells, but rather directly from wild-type euploid cells. These suggests that at the lineage  
level, aneuploidy may be an evolutionary diversion, rather than a stepping stone, on the path to  
76 adaptation.

## Results

78 In the heat-stress experiment of Yona et al.<sup>70</sup>, four populations of *S. cerevisiae* evolved under 39 °C.  
Aneuploidy fixed in all four experimental repetitions in the first 450 generations. Two of the repetitions,  
80 marked *H2* and *H4*, carried no large-scale duplications other than a Chromosome III trisomy. These  
two repetitions continued to evolve under the same conditions, wherein aneuploidy was eliminated by  
82 generation 1,700 and 2,350 in *H4* and *H2*, respectively.

**Evolutionary genetic model.** To explore the dynamics during the evolutionary experiments, we  
84 developed an evolutionary genetic model, fitted the model to empirical data, and used it to predict the  
genotype frequency dynamics, or specifically, the fraction of the evolved euploid population descended  
86 from aneuploid cells.

The model includes the effects of natural selection, genetic drift, aneuploidy, and mutation, and follows  
88 a population of cells characterized by their genotype: euploid wild-type,  $2n$ , is the ancestral diploid  
genotype; euploid mutant,  $2n^*$ , has a diploid karyotype and a single beneficial mutation; aneuploid  
90 wild-type,  $2n+1$ , has an extra chromosome due to a chromosome duplication event; and aneuploid  
mutant,  $2n+1^*$ , has and extra chromosome (like  $2n+1$ ) and a beneficial mutation (like  $2n^*$ ). Fitness  
92 values of the different genotypes are denoted by  $w_{2n}$ ,  $w_{2n^*}$ ,  $w_{2n+1}$ , and  $w_{2n+1^*}$ , and the rate of mutation  
and aneuploidy are denoted by  $\mu$  and  $\delta$ , respectively. See Figure 1 for an illustration of the model.

94 We fitted this model to the experimental results<sup>70</sup> – time for fixation (>95%) and for loss (<5%) of  
aneuploidy – using approximate Bayesian computation with sequential Monte Carlo (ABC-SMC)<sup>59</sup>,

96 thereby inferring the model parameters: rates aneuploidy and mutation and the fitness of all genotypes.  
 We then sampled posterior predictions for the genotype frequency dynamics using the estimated  
 98 parameter values and compared different versions of the model to test additional hypotheses about the evolutionary process.

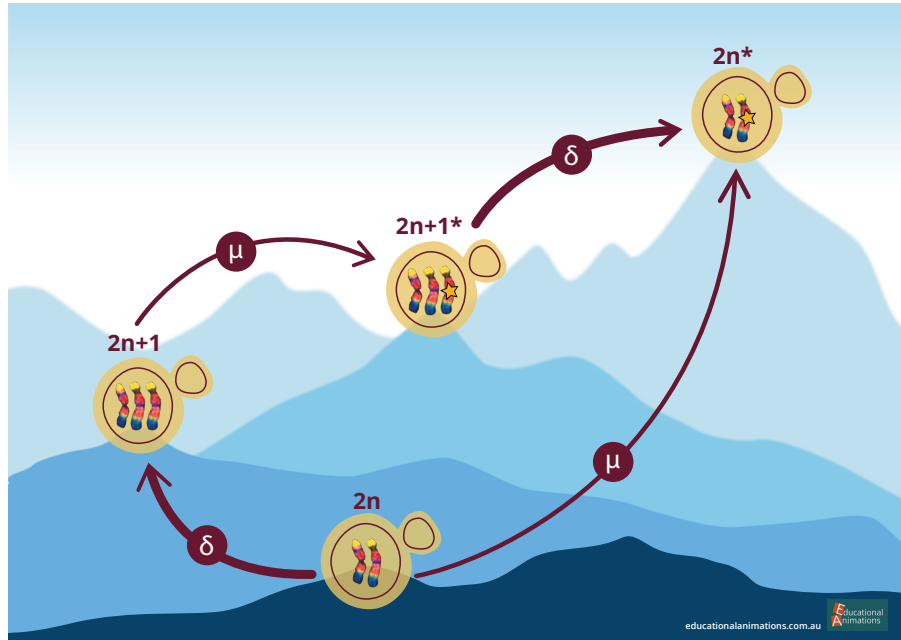


**Figure 1: Model Illustration.** There are four genotypes in our model: euploid wild-type,  $2n$ ; euploid mutant,  $2n^*$ ; aneuploid wild-type,  $2n+1$ ; and aneuploid mutant,  $2n+1^*$ . Overall there are two possible trajectories from  $2n$  to  $2n^*$ . Arrows denote transitions between genotypes, with transitions rates  $\mu$  for the beneficial mutation rate and  $\delta$  for the aneuploidy rate. Elevation differences illustrate the expected, rather than the assumed, fitness differences between the genotypes.

100 **Estimated rates and fitness effects of aneuploidy and mutation.** We inferred the posterior distribution of model parameters (Figure 2). We report parameter estimates using the MAP (maximum a 102 posteriori) and providing the 50% HDI (highest density interval) in square brackets. See Supplementary Material for sensitivity analysis.

104 The estimated beneficial mutation rate is  $\mu = 2.965 \cdot 10^{-6}$  [ $2.718 \cdot 10^{-7} - 3.589 \cdot 10^{-6}$ ] per genome per generation (that is, roughly 3 out of  $10^6$  cell divisions produce a mutant cell with a fitness 106 advantage). From the literature, the mutation rate per base pair is roughly  $2 - 3 \cdot 10^{-10}$  (refs.<sup>74,35</sup>), but it may be higher under heat stress, as several stresses<sup>20</sup>, including heat<sup>22</sup>, may cause hypermutation 108 in yeast. If we assume a 10-fold increase over the mutation rate reported in the literature, then the estimated beneficial mutation rate can be explained by a genomic target size of 1,000 base pairs 110 (that is, 1,000 base pairs across the genome in which a mutation would provide a fitness advantage):  $3 \cdot 10^{-10} \times 10 \times 1,000 = 3 \cdot 10^{-6}$ . Supporting this, Jarolim et al.<sup>25</sup> found 279 genes that contributed

112 to survival after a sudden shift from 30 °C to 50 °C, and Flynn et al.<sup>14</sup> used a deep mutational  
114 scan of a single protein, Hsp90, to find 465 amino-acid variants (out of 14,160) that significantly  
116 increased growth rate in 37 °C. Furthermore, Yona et al.<sup>70</sup> found at least 10 genes on Chromosome  
III that increased heat tolerance when over-expressed. Assuming that other chromosomes also have  
118 a similar number of heat-tolerance genes (and even more, as Chromosome III is one of the smallest  
chromosomes<sup>18</sup>), we get a total of 160 heat-tolerance genes in the genome. Indeed, mutations were  
120 found in 97 genes in an evolutionary experiment with yeast under heat stress<sup>22</sup>. Thus, to get a genomic  
target size of 1,000, it is enough that the average gene target size (number of base pairs in a gene in  
122 which a mutation is beneficial) is 6.25 base pairs. For example, Kohn and Anderson<sup>30</sup> found a target  
size of 11 in a proton exporter gene (*PMA1*) that contributes to high-salt adaptation.

122 The estimated aneuploidy rate,  $\delta = 1.72 \cdot 10^{-3}$  [ $1.47 \cdot 10^{-3} - 2.786 \cdot 10^{-3}$ ] is higher than in previous  
studies: for Chromosome III in diploid *S. cerevisiae*, Zhu et al.<sup>74</sup> estimated  $6.7 \cdot 10^{-6}$  chromosome  
124 gain events per generation, and Kumaran et al.<sup>32</sup> estimate  $3.0 \cdot 10^{-5} - 4.3 \cdot 10^{-5}$  chromosome loss  
events per generation (95% confidence interval). However, this difference may be partly explained  
126 by an increased aneuploidy rate during heat stress: heat shock can increase the rate of chromosome  
fragment loss by 2-3 orders of magnitude<sup>5</sup>.

128 The estimated fitness values are  $w_{2n+1} = 1.022$  [1.021 – 1.023],  $w_{2n+1^*} = 1.025$  [1.024 – 1.026],  
 $w_{2n^*} = 1.028$  [1.026 – 1.029], all relative to the fitness of  $2n$ , which is set to  $w_{2n} = 1$ . If we allow for  
130 transitions (mutation, chromosome loss and gain) to less-fit genotypes (e.g.,  $2n^*$  to  $2n+1^*$ ), then we  
infer similar but slightly different values, see Supplementary Material.

132 **Model comparison and goodness-of-fit.** To assess the fit of our model to the data, we use posterior  
predictive checks, in which we simulate the frequency dynamics using MAP parameter estimates and  
134 compare them to the data. Our model fits the data well:  $2n^*$  fixed in 63% of simulations by generation  
1,700 and in 100% of simulations by generation 2,350 (Figure 3).

136 However, a model without aneuploidy (where the aneuploidy rate is fixed at zero,  $\delta = 0$ ), fails to  
explain the experimental observations (Figure 3). The estimated mutation rate without aneuploidy is  
138  $\mu = 7.98 \cdot 10^{-9}$  [ $7.906 \cdot 10^{-9} - 8.138 \cdot 10^{-9}$ ], much lower compared to a model with aneuploidy. The  
fitness of the mutant is also much lower at  $w_{2n^*} = 1.013$  [1.012 – 1.013]. This is because, without  
140 aneuploidy, a high mutation rate or fitness effect will lead to faster appearance and fixation of  $2n^*$  than  
in the experimental observations.

142 We also checked a model in which aneuploidy occurs but is adaptively neutral compared to the wild-

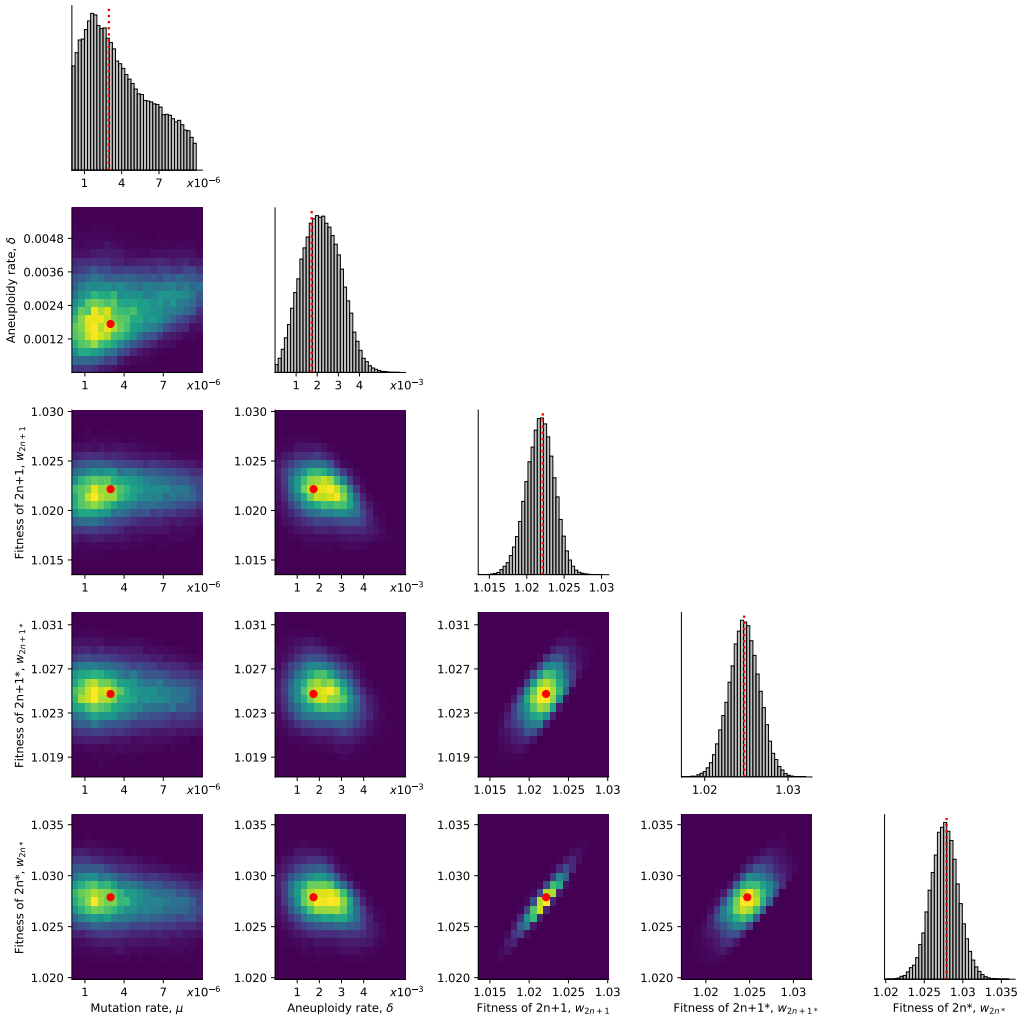


**Figure 2: Posterior distribution of model parameters.** On the diagonal, the marginal posterior distribution of each model parameter. Below the diagonal, the joint posterior distribution of pairs of model parameters (dark purple and bright yellow for low and high density, respectively). Red markers and orange lines for the joint MAP estimate (which may differ from the marginal MAP, as the marginal distribution integrates over all other parameters).

type, that is,  $w_{2n+1} = w_{2n}$  and  $w_{2n+1*} = w_{2n*}$  but  $\delta > 0$ . This model fits the data better than the model  
144 with no aneuploidy (in which  $\delta = 0$ ), but worse than a model with positive selection for aneuploidy,  
in which  $w_{2n} < w_{2n+1} < w_{2n+1*} < w_{2n*}$  (Figure 3).

146 **Model predictions of genotype frequency dynamics.** We simulated 50 replicate genotype frequency dynamics using the MAP estimate parameters. Figure 4A shows the simulated frequencies of  
148 the four genotypes ( $2n$ ,  $2n+1$ ,  $2n+1^*$  and  $2n^*$ ), as well as the frequencies of  $2n^*$  cells that arose from either  $2n+1$  cells via a sequences of mutation and chromosome loss events ( $2n_A^*$ ), or directly from  
150  $2n$  cells via a mutation event ( $2n_M^*$ ). We find that  $2n+1^*$  never reaches substantial frequency as it is quickly replaced by  $2n^*$  in a process similar to *stochastic tunneling*<sup>24,31</sup>.

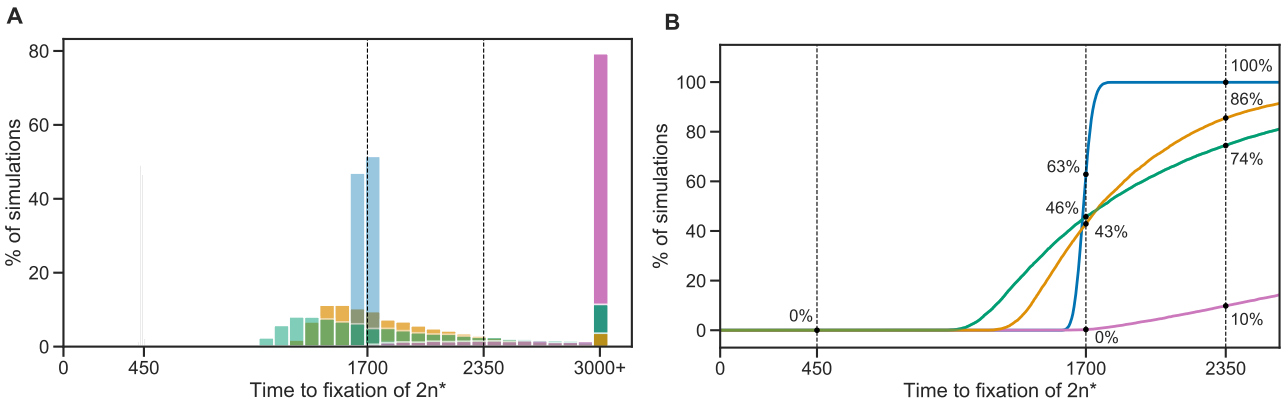


**Figure 3: Model fit with and without aneuploidy.** The distribution of time to fixation of  $2n^*$  (i.e., adaptation time) in 10,000 simulations using MAP parameters of the model with beneficial aneuploidy (blue;  $\delta > 0$ ,  $w_{2n} < w_{2n+1} < w_{2n+1}^* < w_{2n}^*$ ) compared to alternative models: a model with the same parameter values but without aneuploidy (gray,  $\delta = 0$ , concentrated at  $t = 450$ ); a model fitted to the data assuming no aneuploidy (green,  $\delta = 0$ ); a model fitted to the data assuming neutral aneuploidy (yellow,  $\delta > 0$ ,  $w_{2n+1} = w_{2n}$ ,  $w_{2n+1}^* = w_{2n}^*$ ); and a model with beneficial aneuploidy and an extended prior distribution (pink). In the experiment by Yona et al.<sup>70</sup>, one population lost aneuploidy by generation 1,700 and another by generation 2,350 (dashed lines) but not before generation 450. Thus, the blue distribution has a better fit compared to the other distributions (the gray distribution has a particularly poor fit). The MAP likelihood (eq. (4)) is 0.84, 0.78, 0.67, and 0.14 for the models represented by blue, yellow, green, and pink distributions, respectively. **(A)** Histogram of the time to fixation of  $2n^*$ . The last bin contains all values equal or greater than 3,000. **(B)** Cumulative distribution of the time to fixation.

- 152 To test the hypothesis that aneuploidy facilitates adaptation, we estimated  $F_A$ , the expected frequency  
of  $2n^*$  that arose from  $2n+1$ , computed as the average frequency of such  $2n_A^*$  cells at the end of  
154 simulations using the MAP estimate parameters. Surprisingly, we observe that the majority of  $2n^*$   
cells are  $2n_M^*$ , a product of a direct mutation in  $2n$  cells, rather than descending from  $2n+1$  cells  
156 ( $F_A^{MAP} = 0.106$ , average end point of 50 purple lines in Figure 4A). This is despite the fact that the  
2n+1 genotype reaches high frequencies in the population (at least 0.98, Figure 4A).
- 158 This result is not unique to the MAP parameter estimate. We simulated genotype frequency dynamics  
using parameter samples from the posterior distribution, and computed the posterior distribution of  
160  $F_A$  (Figure 4B). The posterior mode  $F_A$  was just 0.147 [0.0154-0.370 95% CI] and only in 489 of  
100,000 posterior samples (0.489%)  $F_A$  was larger than 0.5 (see Supporting Material for results when  
162 transitions to less-fit genotypes are allowed, such as  $2n^*$  to  $2n+1^*$ ). Thus, if we sample a random  
cell from the evolved  $2n^*$  population, it is more likely to have descended directly from an euploid  
164 cell than from an aneuploid cell. The probability of  $2n^*$  descending from  $2n+1$  ( $F_A$ ) increases

with the aneuploidy rate,  $\delta$ , and decreases with both the population size  $N$  and the mutation rate,  $\mu$

166 (Figure 4C,D). In some cases it can also be affected by the fitness parameters (Figure S10).

**Genetic instability in aneuploid cells.** It has been suggested that aneuploidy increases genetic

168 instability: Sheltzer et al.<sup>56</sup> have demonstrated a fold increase of between 2.2 and 7.1 in mutation

rate. Therefore, we inferred model parameters under the assumption that the mutation rate increases

170 in aneuploid cells by a factor  $\tau = 1, 33/32$  (due to an additional chromosome), 2, 5, 10, or 100 (due

to genetic instability). We found that the posterior distribution was similar for  $\tau = 1, 33/32, 2$ , and 5

172 (Figure S4). Furthermore, we computed the WAIC, a criterion for model selection (Methods). The

WAIC values were similar for all  $\tau$  values (Table S1).

174 Assuming a strong increase of the mutation rate in aneuploid cells, i.e.  $\tau = 100$ , the inferred a

mutation rate was  $\mu = 4.094 \cdot 10^{-7}$  [ $6.252 \cdot 10^{-8} - 6.046 \cdot 10^{-7}$ ]), and the inferred aneuploidy rate

176 that was  $\delta = 0.744 \cdot 10^{-3}$  [ $0.506 \cdot 10^{-3} - 1.827 \cdot 10^{-3}$ ]. Compared to inference made assuming no

effect of aneuploidy on the mutation rate, these rates were about 7-8-fold and 2-3-fold lower for  $\mu$  and

178  $\delta$ , respectively. Assuming  $\tau = 10$ , the inferred a mutation rate was only slightly lower compared to

$\tau = 1$  ( $\mu = 1.67 \cdot 10^{-6}$  [ $2.836 \cdot 10^{-8} - 2.245 \cdot 10^{-6}$ ]).

180 Therefore, we do not find any evidence of an increase in mutation rate in aneuploid cells. This may

be because, unless the increase is strong ( $\tau \geq 10$ ), it does not seem to affect our inference; or because

182 Chromosome III is one of the smallest chromosomes<sup>18</sup>. We also checked the differences in genotype

frequency dynamics for different  $\tau$  values. We observe  $\tau = 100$  could be distinguished if accurate

184 data was available for the waiting time until the frequency of  $2n$  to decrease below 95% (Figure S5A)

or for waiting time for the frequency of  $2n+1$  to either reach or go below 95% (Figure S5B). Similarly,

186 we did not find evidence for an increase in the rate of chromosome loss in aneuploid cells<sup>56</sup>, probably

due to lack of statistical power.

188 Nevertheless, increasing the rate of chromosome loss (transitions from  $2n+1^*$  to  $2n^*$ ) without increasing

the rate of chromosome gain (transitions from  $2n$  to  $2n + 1$ ) increases  $F_A$  (Figure S11B), but not to the

190 same extent as increasing the rate of chromosome gain. In contrast, increasing the mutation rate in

aneuploid cells can have a marked effect on the dynamics: when using the MAP parameter estimates,

192  $F_A$  increases to 0.52 when the mutation rate in aneuploid cells increases 10-fold (Figure S11C).

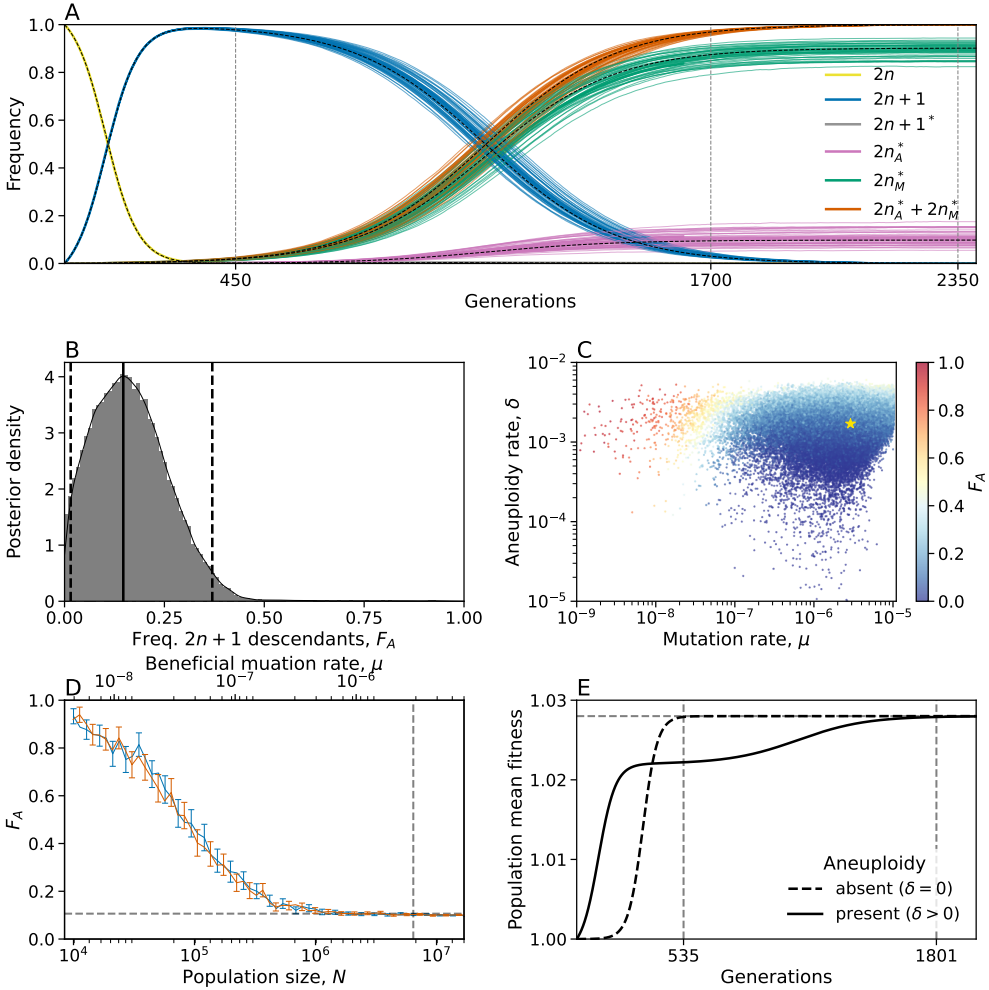


**Figure 4: Predicted frequency of aneuploid-descended cells.** **(A)** Posterior predicted genotype frequencies over time, including the source of  $2n^*$ :  $2n_A^*$  arose from  $2n + 1$ , whereas  $2n_M^*$  arose directly from  $2n$ . Colored curves are 50 simulations using the MAP estimate parameters. Black dashed curves are the expected genotype frequencies without genetic drift (from a deterministic model). See Figure S9 for log-log scale, in which the sequence of events is easier to observe. **(B)** Posterior distribution of  $F_A$ , the expected frequency of  $2n^*$  cells descended from  $2n+1$  cells, computed as the average frequency at the end of 100 simulations for 100,000 samples from the parameter posterior distribution. Solid and dashed lines show the mode and 95% CI. **(C)**  $F_A$  values (color coded) from panel B, with their corresponding mutation rate  $\mu$  on x-axis and aneuploidy rate  $\delta$  on the y-axis. Yellow star shows the MAP estimate. See also Figure S10. **(D)**  $F_A$  as a function of the population size ( $N$ , bottom x-axis) and the beneficial mutation rate ( $\mu$ , top x-axis) in posterior predictions with MAP parameters. Markers show  $F_A$  in 250 simulations per population size or mutation rate value. Error bars show mean  $F_A$  with 95% CI (bootstrap,  $n = 10,000$ ). Blue and red bars for varying population size and mutation rate, respectively. Vertical dashed line for population size in the experiment,  $6.425 \cdot 10^6$ , and the MAP mutation rate,  $2.965 \cdot 10^{-6}$ . Horizontal line for  $F_A^{MAP} = 0.106$ . **(E)** Population mean fitness in a model without drift using MAP estimate parameters. Solid lines for mean fitness with aneuploidy ( $\delta > 0$ ), where the population reaches adaptation (mean fitness at 99.99% of maximum value) at generation 1,802. Dashed lines for mean fitness without aneuploidy ( $\delta = 0$ ), where the population adapts much earlier, at generation 535.

## Discussion

194 In a study on the role of chromosome duplication in adaptive evolution, Yona et al.<sup>70</sup> found that a  
195 Chromosome III trisomy was acquired by *S. cerevisiae* populations evolving under heat stress, only  
196 to be later replaced by euploid mutant cells that carry "refined" solutions to the stress. Additionally,  
197 such a replacement also occurred when they initiated evolutionary experiments with a population in  
198 which all cells carry a Chromosome III trisomy. They hypothesized that aneuploidy is a "useful yet  
199 short-lived intermediate that facilitates further adaptation", suggesting that the euploid mutant cells  
200 evolved by heat-resistance mutations in aneuploid cells followed by reversion of trisomy due to a  
201 chromosome loss event.

202 We developed an evolutionary genetic model of adaptive evolution by aneuploidy and mutation  
(Figure 1), fitted it to the experimental results of Yona et al.<sup>70</sup>, and used it to predict the genotype  
204 frequency dynamics. The model predicted that only about 10-15% of the evolved euploid population  
descended from aneuploid cells by acquiring a mutation and losing the extra chromosome—that is,  
206 the majority of the euploid population are not descended from aneuploid cells, but rather are direct  
descendants of the ancestral wild-type population (Figure 4).

208 This happens despite aneuploidy reaching a high frequency in the population (>95%). Conventional  
wisdom might suggest that once the aneuploid genotype  $2n+1$  reaches high frequency, it will have a  
210 better chance at producing "refined" solutions via mutations, and its descendants will come to dominate  
the population: the frequency of  $2n_A^*$  (which arises from  $2n+1^*$ ) will be higher than the frequency of  
212  $2n_M^*$  (which arises directly from  $2n$ ).

So how does  $2n_M^*$  prevail? Initially, the supply rates of  $2n+1$  and  $2n_M^*$  are  $N\delta \approx 11,000$  and  $N\mu \approx 19$ ,  
214 respectively (assuming MAP parameter estimates). Therefore, both genotypes are expected to appear  
immediately at the beginning of the experiment (Figure S9). However,  $2n+1$  appears at a much higher  
216 frequency as  $\delta \gg \mu$  by 2-3 orders of magnitude. After they first appear,  $2n_M^*$  has higher fitness. But  
as long as the frequency of  $2n$  is high, the supply rate of  $2n+1$  is higher than that of  $2n_M^*$ , again due to  
218  $\delta \gg \mu$ . However, supply rates of both genotypes decrease with the frequency of  $2n$ . Therefore, when  
the latter decreases, mainly due to the increase in the frequency of  $2n+1$ , both supply rates diminish.  
220 At this stage, the higher fitness of  $2n_M^*$  comes into play and it starts to take over the population, which  
is mainly composed of  $2n+1$ . For the aneuploid lineage to compete with the mutant lineage, it must  
222 produce  $2n_A^*$  via a mutation followed by chromosome loss. Although this is a stochastic process  
(due to drift), our results show that the time until  $2n_A^*$  reaches a frequency of 0.1% is roughly 450  
224 generations, without much variation (intersection of purple lines and vertical dashed line in Figure S9).

However, by that time  $2n_M^*$  is already at a roughly 10-fold higher frequency (1.86%), and since both mutants have the same fitness, their relative frequency remains roughly the same until the end of the experiment.

**Predictions for small populations and low mutation rates.** We examined the effect of the population size,  $N$ , and the beneficial mutation rate,  $\mu$ , on the frequency of  $2n+1$  descendants in the evolved population,  $F_A$ . We found that  $F_A$  is expected to decrease as the population size or mutation rate increase (Figure 4D), ranging from >90% when the population size is 10,000 or the mutation rate is  $6 \cdot 10^{-9}$ , to about 10% when the population size is above 1,000,000 (less than the experimental population size, which was 6,425,000) or the mutation rate is above  $2 \cdot 10^{-6}$  (less than the inferred mutation rate, which is  $2.965 \cdot 10^{-6}$ ). Thus, our model provides a testable prediction: if the experiment was repeated under a lower population size (via stronger daily dilutions or in a smaller volume) or a lower mutation rate (via a non-mutagenic stress or stress with a smaller target size such as drug resistance), then the fraction of the population descending from aneuploid cells would be much higher.

**Aneuploidy delays rather than facilitates adaptation.** An additional interesting result of our study is that aneuploidy increases, rather than decreases, the adaptation time (Figure 4E). This happens despite the fact that the mean fitness initially increases faster in the presence of aneuploidy (Figure 4E). This is because once  $2n+1$  is common, selection for the mutant strain ( $2n+1^*$  or  $2n^*$ ) is weaker compared to when  $2n^*$  competes directly with  $2n$ .

**Rate and fitness effect of aneuploidy and mutation.** We inferred the rates of aneuploidy and mutation and their effects on fitness. We estimate that the aneuploidy rate (i.e., number of chromosome gains per generation) is  $1.7 \cdot 10^{-3}$ , higher than a previous estimate of  $6.7 \cdot 10^{-6}$  (ref<sup>73</sup>). This may be due to genetic instability caused by heat stress<sup>5</sup>. In addition, we find no evidence for increased mutation rates in aneuploid cells. Previous empirical studies have suggested that genetic instability (e.g., elevated mutation rates) in aneuploid cells is due to stress associated with the aneuploid state<sup>3,6,71,23</sup>. However, in the experiment of Yona et al.<sup>70</sup>, both the wild-type and the aneuploid were under heat stress, which may explain why we did not find evidence for an increased mutation rate specifically in aneuploid cells.

**Conclusions.** Here, we tested the hypothesis that aneuploidy cells are an evolutionary "stepping stone", or adaptive intermediate, between wild-type euploid cells and mutant euploid cells<sup>69</sup>. Our results suggest that, although it seems the population goes from euploid to aneuploid and back, this is not the case at the individual level. We estimate that only about 10-15% of the euploid cells descended

256 from aneuploid cells, whereas the rest are direct descendants of the wild-type euploid cells. Thus,  
257 aneuploidy can delay, rather than accelerate, adaptation, and cells that become aneuploid may leave  
258 less descendants than cells that remain euploid. This surprising result reinforces the importance of  
259 mathematical models when interpreting evolutionary dynamics. Moreover, our study emphasizes the  
260 unintuitive outcomes of clonal interference between mechanisms for generation of variation that differ  
261 in their rate of formation and distribution of fitness effects, including mutation, copy number variation,  
262 horizontal gene transfer, and epigenetic modifications.

## Models and Methods

264 **Evolutionary genetic model.** We model the evolution of a population of cells using a Wright-  
265 Fisher model<sup>40</sup>, assuming a constant effective population size  $N$ , non-overlapping generations, and  
266 including the effects of natural selection, genetic drift, aneuploidy, and mutation. We focus on bene-  
267 ficial genetic modifications, neglecting the effects of deleterious and neutral mutations or karyotypic  
268 changes. The model allows for a single aneuploid karyotype (e.g., Chromosome III duplication) and  
269 a single mutation to accumulate in the genotype. Thus, the model follows four genotypes (Figure 1):  
270 euploid wild-type,  $2n$ , the initial genotype; euploid mutant,  $2n^*$ , with the standard karyotype and  
271 a single beneficial mutation; aneuploid wild-type,  $2n+1$ , with an extra chromosome, i.e., following  
272 chromosome duplication; and aneuploid mutant,  $2n+1^*$ , with an extra chromosome and a beneficial  
273 mutation.

274 Transitions between the genotypes occur as follows (Figure 1): Beneficial mutations from  $2n$  to  $2n^*$   
275 and from  $2n+1$  to  $2n+1^*$  occur with probability  $\mu$ , the mutation rate. We neglect back-mutations (i.e.,  
276 from  $2n^*$  to  $2n$  and from  $2n+1^*$  to  $2n+1$ ). Aneuploidy is formed by chromosome mis-segregation,  
277 so that cells transition from  $2n$  to  $2n+1$  and from  $2n+1^*$  to  $2n^*$  with probability  $\delta$ , the aneuploidy  
278 rate. That is, we assume chromosomes are gained and lost at the same rate, and we neglect events that  
279 form a less-fit genotype (i.e.,  $2n+1$  to  $2n$  and  $2n^*$  to  $2n+1^*$ ). A model that assumed increased rate  
280 of chromosome loss in aneuploid cells (as in Sheltzer et al.<sup>56</sup>) did not perform well, probably due to  
281 lack of statistical power, and was abandoned.

282 In the experiment by Yona et al.<sup>70</sup>, the population was grown every day from  $1.6 \cdot 10^6$  cells until  
283 reaching stationary phase and then diluted 1:120. Thus, we set the population size to  $N = 6.425 \cdot 10^6$ ,  
284 the harmonic mean of  $\{2^k \cdot 1.6 \cdot 10^6\}_{k=0}^7$ <sup>10</sup>. The initial population has  $N$  cells with genotype  $2n$ .  
285 The effect of natural selection on the frequency  $f_i$  of genotype  $i = 2n, 2n + 1, 2n + 1^*$ , or  $2n^*$  is given

286 by

$$f_i^s = \frac{f_i w_i}{\bar{w}}, \quad (1)$$

288 where  $w_i$  is the fitness of genotype  $i$  and  $\bar{w} = \sum_j f_j w_j$  is the population mean fitness. The effect of mutation and aneuploidy on genotype frequencies is given by

$$\begin{aligned} 290 \quad f_{2n}^m &= (1 - \delta - \mu) f_{2n}^s, \\ f_{2n+1}^m &= \delta f_{2n}^s + (1 - \mu) f_{2n+1}^s, \\ f_{2n+1^*}^m &= \mu f_{2n+1}^s + (1 - \delta) f_{2n+1^*}^s, \\ f_{2n^*}^m &= \mu f_{2n}^s + \delta f_{2n+1^*}^s + f_{2n^*}^s. \end{aligned} \quad (2)$$

Finally, random genetic drift is modeled using a multinomial distribution<sup>40</sup>,

$$292 \quad \mathbf{f}' \sim \frac{1}{N} \cdot \text{Mult}(N, \mathbf{f}^m), \quad (3)$$

where  $\mathbf{f}^m = (f_{2n}^m, f_{2n+1}^m, f_{2n+1^*}^m, f_{2n^*}^m)$  are the frequencies of the genotypes after mutation and  
294 aneuploidy,  $\mathbf{f}'$  are the genotype frequencies in the next generation, and  $\text{Mult}(N, \mathbf{f})$  is a multinomial  
distribution parameterized by the population size  $N$  and the genotype frequencies  $\mathbf{f}$ . Overall, the change  
296 in genotype frequencies from one generation to the next is given by the transformation  $f_i \rightarrow f'_i$ .

**Empirical data for model inference.** We use the results of evolutionary experiments reported by

298 Yona et al.<sup>70</sup>. In their heat-stress experiment, four populations of *S. cerevisiae* evolved under 39 °C.  
Aneuploidy fixed in all four population in the first 450 generations. Hereafter, fixation or elimination  
300 of a genotype *by generation t* means that more than 95% or less than 5% of the population carry  
the genotype at generation  $t$ , and possibly earlier. In the original analysis of Yona et al.<sup>70</sup>, samples  
302 were routinely extracted from the evolving populations and tested for heat-shock tolerance. The first  
generation in which such indication was found was generation 200. Therefore, we determine that  
304 aneuploidy did not fix before generation 200. The experiment continued with two populations, in  
which aneuploidy was eliminated by generation 1,700 and 2,350 while still under the same conditions  
306 of elevated heat (39 °C).

**Likelihood function.** Because our model, just like the Wright-Fisher model, is non-linear and

308 stochastic, computing the distribution of fixation time  $T(g)$  of genotype  $g$  for use in the likelihood  
function is intractable (it is even hard to use a diffusion-equation approximation due to the model having  
310 multiple genotypes, rather than just two). We overcome this problem by approximating the likelihood  
using simulations. We simulate 1,000 experiments per parameter vector  $\theta = (\mu, \delta, s, b, c)$ , resulting

312 in a set of simulated observations  $\tilde{\mathbf{X}} = \{\tilde{X}_i\}_{i=1}^{1000}$ . We then compute the approximate likelihood,

$$\begin{aligned}\mathcal{L}(\theta) = P^4(200 \leq T(2n+1) \leq 450) \cdot & \left[ 1 - \right. \\ & P_{\tilde{\mathbf{X}}}^4(\{T(2n^*) < 1700\} \mid 200 \leq T(2n+1) \leq 450) - \\ & P_{\tilde{\mathbf{X}}}^4(\{1700 < T(2n^*) < 2350\} \mid 200 \leq T(2n+1) \leq 450) + \\ & \left. P_{\tilde{\mathbf{X}}}^4(\{T(2n^*) < 1700\} \wedge \{1700 < T(2n^*) < 2350\} \mid 200 \leq T(2n+1) \leq 450) \right],\end{aligned}\tag{4}$$

314 where  $!\{\dots\}$  is the "logical not" operator,  $P^4(\dots)$  is the 4th power of  $P(\dots)$ , and all probabilities  
 $P_{\tilde{\mathbf{X}}}(\dots)$  are approximated from the results of the simulations  $\tilde{\mathbf{X}}$ . For example,  $P_{\tilde{\mathbf{X}}}(\{T(2n^*) < 1700\} \mid$   
316  $200 \leq T(2n+1) \leq 450)$  is approximated by taking simulations in which  $2n+1$  fixed before generation  
450 but not before generation 200, and computing the fraction of such simulations in which  $2n^*$  did  
318 not fix by generation 1,700, and hence aneuploidy did not extinct before generation 1,700. Figure S1  
compares results with less and more simulated experiments, demonstrating that 1,000 simulations are  
320 likely sufficient.

For a model without aneuploidy (that is, when the aneuploidy rate is fixed at zero,  $\delta = 0$ ), we disregard  
322 the increased expression in Chromosome III and the growth advantage measured in generation 450,  
and focus on the growth advantage measured in later generations, presumably due to a beneficial  
324 mutation. Therefore, the likelihood is approximated by

$$\begin{aligned}\mathcal{L}_!(\theta) = 1 - & P_{\tilde{\mathbf{X}}}^4(\{T(2n^*) < 1700\}) - \\ & P_{\tilde{\mathbf{X}}}^4(\{1700 < T(2n^*) < 2350\}) + \\ & P_{\tilde{\mathbf{X}}}^4(\{T(2n^*) < 1700\} \wedge \{1700 < T(2n^*) < 2350\}).\end{aligned}\tag{5}$$

326 **Parameter inference.** To infer model parameters, we use approximate Bayesian computation with  
a sequential Monte-Carlo scheme, or ABC-SMC<sup>59</sup>, implemented in the pyABC Python package<sup>29</sup>  
328 [pyabc.readthedocs.io](#). This approach uses numerical stochastic simulations of the model to infer  
a posterior distribution over the model parameters. It is a method of likelihood-free, simulation-  
330 based inference<sup>9</sup>, that is, for estimating a posterior distribution when a likelihood function cannot be  
directly computed. It is therefore suitable in our case, in which the likelihood function can only be  
332 approximated from simulations, and cannot be directly computed.

The ABC-SMC algorithm employs sequential importance sampling over multiple iterations<sup>63,28,61</sup>. In  
334 iteration  $t$  of the algorithm, a set of parameter vectors,  $\{\theta_{i,t}\}_{i=1}^{n_t}$ , also called *particles*, are constructed  
in the following way. A proposal particle,  $\theta^*$ , is sampled from a proposal distribution, and is either  
336 accepted or rejected, until  $n_t$  particles are accepted. The number of particles,  $n_t$ , is adapted at every  
iteration  $t$  using the adaptive population strategy<sup>29</sup> [pyabc.readthedocs.io](#). For  $t = 0$ , the proposal

338 particle is sampled from the prior distribution,  $p(\theta)$ . For  $t > 0$ , the proposal particle is sampled from  
 339 the particles accepted in the previous iteration,  $\{\theta_{i,t-1}\}_{i=1}^{n_{t-1}}$ , each with a probability relative to its weight  
 340  $W_{t-1}(\theta_{i,t-1})$  (see below). The proposal particle is then perturbed using a kernel perturbation kernel,  
 341  $K_t(\theta^* | \theta)$  where  $\theta$  is the sample from the previous iteration. Then, a set of synthetic observations  
 342  $\tilde{\mathbf{X}}^*$  is simulated, and the proposal particle  $\theta^*$  is accepted if its approximate likelihood (eq. (4)) is high  
 343 enough,  $\mathcal{L}(\theta^*) > 1 - \epsilon_t$  (or more commonly, if  $1 - \mathcal{L}(\theta^*) < \epsilon_t$ ), where  $\epsilon_t > 0$  is the *acceptance*  
 344 *threshold*, as higher values of  $\epsilon_t$  allow more particles to be accepted. The acceptance threshold  $\epsilon_t$  is  
 345 chosen as the median of the  $1 - \mathcal{L}(\theta)$  of the particles accepted in the previous iteration,  $t - 1$ , and  
 346  $\epsilon_0 = 0.01$ . For each accepted particle  $\theta_{i,t}$  a weight  $W_t(\theta_{i,t})$  is assigned: for  $t = 0$ ,  $W_0(\theta_{i,0}) = 1$ ,  
 347 and for  $t > 0$ ,  $W_t(\theta_{i,t}) = p(\theta_{i,t}) / \sum_{i=1}^{n_{t-1}} W_{t-1}(\theta_{i,t-1}) K_t(\theta_{i,t}, \theta_{i,t-1})$ , where  $p(\theta)$  is the prior density of  
 348  $\theta$  and  $K_t(\theta', \theta)$  is the probability of a perturbation from  $\theta$  to  $\theta'$ .  $K_t(\theta' | \theta)$  is a multivariate normal  
 349 distribution, fitted at iteration  $t$  to the particles from the previous iteration,  $\{\theta_{i,t-1}\}_{i=1}^{n_{t-1}}$ , and their  
 350 weights,  $\{W(\theta_{i,t-1})\}_{i=1}^{n_{t-1}}$ .

Acceptance is determined according to the approximate likelihood (eq. (4)), which has a maximum  
 351 value of  $\mathcal{L}_{max} = 0.875$  (giving a minimal value of  $\epsilon_{min} = 0.125$ ). We terminated the inference  
 352 iterations when the change in  $\epsilon$  value from one iteration to the next was small. With our standard prior  
 353 and model, we reached  $\epsilon = 0.13$  (or  $\mathcal{L} = 0.87$ ) after six iterations, with  $n_6 = 982$  accepted parameter  
 354 vectors and effective sample size ESS=651 (Figure S2). Running the inference algorithm with different  
 355 initialization seeds and less or more simulations for approximating the likelihood produced similar  
 356 posterior distributions (Figure S1).

357 After producing a set of weighted particles from the the posterior distribution using the above ABC-  
 358 SMC algorithm, we approximate the posterior using kernel density estimation (KDE) with Gaussian  
 359 kernels. We truncate the estimated posterior to avoid positive posterior density for values with zero  
 360 prior density. The MAP (maximum a posteriori) estimate is computed as the the maximum of the  
 361 estimated joint posterior density. We then draw 5,000,000 samples from the posterior distribution  
 362 to compute the HDI (highest density interval) and draw 50,000 samples to visualize the posterior  
 363 distribution with histograms.

**Model comparison.** We examine several versions of our evolutionary models, e.g. without aneu-  
 364 ploidy or with increased mutation rate in aneuploid cells, as well as several different prior distributions  
 365 (see below). To compare these, we plot posterior predictions: for each model we execute 10,000  
 366 simulations using the MAP parameter estimates and plot the distributions of time to fixation of  $2n^*$ ,  
 367 one of key properties of the model likelihood. These plots visualize the fit of each model to the

370 data. Also, for similar models we plot the marginal and joint posterior distributions of the parameters;  
if these are similar, we consider the models interchangeable. We validate this by comparing HDI  
372 (highest density interval) of posterior distributions.

Where posterior plots are very similar and the number of parameters is the same, we use WAIC, or  
374 the widely applicable information criterion<sup>15</sup>, defined as

$$WAIC(\theta) = -2 \log \mathbb{E}[\mathcal{L}(\theta)] + 2\mathbb{V}[\log \mathcal{L}(\theta)] \quad (6)$$

376 where  $\theta$  is a parameter vector, and  $\mathbb{E}[\cdot]$  and  $\mathbb{V}[\cdot]$  are the expectation and variance taken over the  
posterior distribution, which in practice are approximated using 50,000 samples from the posterior  
378 KDE. We validated that upon resampling WAIC values do not significantly change and that differences  
in WAIC between models are preserved. WAIC values are scaled as a deviance measure: lower values  
380 imply higher predictive accuracy.

**Prior distributions.** We used informative prior distributions for  $w_{2n+1}$ ,  $w_{2n+1*}$  and  $w_{2n*}$  (we set  
382  $w_{2n} = 1$ ), which we estimated from growth curves data from mono-culture growth experiments  
previously reported by Yona et al.<sup>70</sup>, Figs. 3C, 4A, and S2. We used Curveball, a method  
384 for predicting results of competition experiments from growth curve data<sup>43</sup> [curveball.yoavram.com](http://curveball.yoavram.com).  
Briefly, Curveball takes growth curves of two strains growing separately in mono-culture and predicts  
386 how they would grow in a mixed culture, that is, it predicts the results of a competition assay. From these  
predictions, relative fitness values can be computed. Because Curveball uses a maximum-likelihood  
388 approach to estimate model parameters, we were able to estimate a distribution of relative fitness  
values to be used as a prior distribution by sampling 10,000 samples from a truncated multivariate  
390 normal distribution defined by the maximum-likelihood covariance matrix (Figure S3).

We used growth curves of  $2n$  and  $2n+1$  in 39 °C to estimate an informative prior distribution for  
392  $w_{2n+1}$  (Figure S3D, assuming  $w_{2n} = 1$ ). In this prior distribution, we used the same prior for  $w_{2n+1*}$   
and  $w_{2n*}$ . To increase computational efficiency, we also assumed  $w_{2n*} > w_{2n+1*} > w_{2n+1} > w_{2n}$ ;  
394 running the inference without this assumption produced similar results. See *supporting material* for  
an extended informative prior distribution that uses growth curves of  $2n^*$  and  $2n+1$  growing in 39 °C;  
396 this prior distribution proved to be less useful.

As a control, we tested an uninformative uniform prior with  $U(1, 6)$ , for (i) all  $w_{2n+1}$ ,  $w_{2n+1*}$ ,  $w_{2n*}$ ,  
398 or (ii) only for  $w_{2n+1*}$ ,  $w_{2n*}$ , using the above informative prior for  $w_{2n+1}$ . In these cases the inference  
algorithm failed to converge.

400 For the mutation rate,  $\mu$ , and aneuploidy rate,  $\delta$ , we used uninformative uniform priors,  $\mu \sim$

$U(10^{-9}, 10^{-5})$  and  $\delta \sim U(10^{-6}, 10^{-2})$ . A wider mutation rate prior,  $\mu \sim U(10^{-9}, 10^{-3})$ , produced

402 similar results.

## Acknowledgements

404 We thank Lilach Hadany, Judith Berman, David Gresham, Shay Covo, Martin Kupiec, Uri Obolski, Daniel  
Weissman, and Tal Simon for discussions and comments. This work was supported in part by the Israel  
406 Science Foundation (ISF, YR 552/19), the US-Israel Binational Science Foundation (BSF, YR 2021276),  
Minerva Center for Live Emulation of Evolution in the Lab (YR, YP), Minerva Stiftung short-term research  
408 grant (MP).

## References

- 410 [1] Avecilla, G., Chuong, J. N., Li, F., Sherlock, G., Gresham, D. and Ram, Y. 2022, ‘Neural  
networks enable efficient and accurate simulation-based inference of evolutionary parameters  
412 from adaptation dynamics’, *PLOS Biology* **20**(5), e3001633.
- 414 [2] Bakhoum, S. F. and Landau, D. A. 2017, ‘Chromosomal instability as a driver of tumor hetero-  
geneity and evolution’, *Cold Spring Harb. Perspect. Med.* **7**(6), 1–14.
- 416 [3] Bouchonville, K., Forche, A., Tang, K. E. S., Semple, C. a. M. and Berman, J. 2009, ‘Aneuploid  
chromosomes are highly unstable during dna transformation of *Candida albicans*.’, *Eukaryot.  
Cell* **8**(10), 1554–66.
- 418 [4] Boveri, T. 2008, ‘Concerning the origin of malignant tumours’, *J. Cell Sci.* **121**(Supplement  
1), 1–84.
- 420 [5] Chen, G., Bradford, W. D., Seidel, C. W. and Li, R. 2012, ‘Hsp90 stress potentiates rapid cellular  
adaptation through induction of aneuploidy.’, *Nature* **482**(7384), 246–50.
- 422 [6] Chen, G., Rubinstein, B. and Li, R. 2012, ‘Whole chromosome aneuploidy: Big mutations drive  
adaptation by phenotypic leap’, *BioEssays* **34**(10), 893–900.
- 424 [7] Cherry, J. M., Hong, E. L., Amundsen, C., Balakrishnan, R., Binkley, G., Chan, E. T., Christie,  
K. R., Costanzo, M. C., Dwight, S. S., Engel, S. R. et al. 2012, ‘Saccharomyces genome database:  
426 the genomics resource of budding yeast’, *Nucleic acids research* **40**(D1), D700–D705.
- [8] Covo, S., Puccia, C. M., Argueso, J. L., Gordenin, D. A. and Resnick, M. A. 2014, ‘The sister

- 428 chromatid cohesion pathway suppresses multiple chromosome gain and chromosome amplification.’, *Genetics* **196**(2), 373–384.
- 430 [9] Cranmer, K., Brehmer, J. and Louppe, G. 2020, ‘The frontier of simulation-based inference’, *Proceedings of the National Academy of Sciences* p. 201912789.
- 432 [10] Crow, J. F. and Kimura, M. 1970, *An introduction to population genetics theory*, Burgess Pub. Co., Minneapolis.
- 434 [11] Dhar, R., Sägesser, R., Weikert, C., Yuan, J. and Wagner, A. 2011, ‘Adaptation of *Saccharomyces cerevisiae* to saline stress through laboratory evolution.’, *J. Evol. Biol.* **24**(5), 1135–53.
- 436 [12] Dunham, M. J., Badrane, H., Ferea, T., Adams, J., Brown, P. O., Rosenzweig, F. and Botstein, D. 2002, ‘Characteristic genome rearrangements in experimental evolution of *Saccharomyces cerevisiae*’, *Proc. Natl. Acad. Sci.* **99**(25), 16144–16149.
- 438 [13] Elde, Nels, C., Child, Stephanie, J., Eickbush, Michael, T., Kitzman, Jacob, O., Rogers, Kelsey, S., Shendure, J., Geballe, Adam, P. and Malik, Harmit, S. 2012, ‘Poxviruses deploy genomic accordions to adapt rapidly against host antiviral defenses’, *Cell* **150**(4), 831–841.
- 440 [14] Flynn, J. M., Rossouw, A., Cote-Hammarlof, P., Fragata, I., Mavor, D., Hollins, C., Bank, C. and Bolon, D. N. 2020, ‘Comprehensive fitness maps of hsp90 show widespread environmental dependence’, *Elife* **9**, 1–25.
- 444 [15] Gelman, A., Carlin, J. B., Stern, H. S., Dunson, D. B., Vehtari, A. and Rubin, D. B. 2013, *Bayesian Data Analysis, Third Edition*, Chapman & Hall/CRC Texts in Statistical Science, Taylor & Francis.
- 448 [16] Gerstein, A. C. and Berman, J. 2020, ‘*Candida albicans* genetic background influences mean and heterogeneity of drug responses and genome stability during evolution in fluconazole’, *mSphere* **5**(3).
- 450 [17] Gerstein, A. C., Ono, J., Lo, D. S., Campbell, M. L., Kuzmin, A. and Otto, S. P. 2015, ‘Too much of a good thing: the unique and repeated paths toward copper adaptation.’, *Genetics* **199**(2), 555–71.
- 454 [18] Gilchrist, C. and Stelkens, R. 2019, ‘Aneuploidy in yeast: Segregation error or adaptation mechanism?’, *Yeast* **36**(9), 525–539.
- 456 [19] Gresham, D., Desai, M. M., Tucker, C. M., Jenq, H. T., Pai, D. A., Ward, A., DeSevo, C. G.,

- Botstein, D. and Dunham, M. J. 2008, ‘The repertoire and dynamics of evolutionary adaptations to controlled nutrient-limited environments in yeast’, *PLoS Genet.* **4**(12).
- [20] Heidenreich, E. 2007, ‘Adaptive Mutation in *Saccharomyces cerevisiae*’, *Crit. Rev. Biochem. Mol. Biol.* **42**(4), 285–311.
- [21] Hong, J. and Gresham, D. 2014, ‘Molecular specificity, convergence and constraint shape adaptive evolution in nutrient-poor environments’, *PLoS Genet.* **10**(1).
- [22] Huang, C. J., Lu, M. Y., Chang, Y. W. and Li, W. H. 2018, ‘Experimental Evolution of Yeast for High-Temperature Tolerance’, *Mol. Biol. Evol.* **35**(8), 1823–1839.
- [23] Ippolito, M. R., Martis, V., Martin, S., Tijhuis, A. E., Hong, C., Wardenaar, R., Dumont, M., Zerbib, J., Spierings, D. C., Fachinetti, D., Ben-David, U., Foijer, F. and Santaguida, S. 2021, ‘Gene copy-number changes and chromosomal instability induced by aneuploidy confer resistance to chemotherapy’, *Dev. Cell* **56**(17), 2440–2454.e6.
- [24] Iwasa, Y., Michor, F. and Nowak, M. A. 2004, ‘Stochastic tunnels in evolutionary dynamics’, *Genetics* **166**(3), 1571–1579.
- [25] Jarolim, S., Ayer, A., Pillay, B., Gee, A. C., Phrakaysone, A., Perrone, G. G., Breitenbach, M. and Dawes, I. W. 2013, ‘*Saccharomyces cerevisiae* genes involved in survival of heat shock’, *G3 Genes, Genomes, Genetics* **3**(12), 2321–2333.
- [26] Kass, R. E. and Raftery, A. E. 1995, ‘Bayes factors’, *J. Am. Stat. Assoc.* **90**(430), 773.
- [27] Kasuga, T., Bui, M., Bernhardt, E., Swiecki, T., Aram, K., Cano, L. M., Webber, J., Brasier, C., Press, C., Grünwald, N. J., Rizzo, D. M. and Garbelotto, M. 2016, ‘Host-induced aneuploidy and phenotypic diversification in the sudden oak death pathogen *Phytophthora ramorum*’, *BMC Genomics* **17**(1), 1–17.
- [28] Klinger, E. and Hasenauer, J. 2017, A scheme for adaptive selection of population sizes in approximate bayesian computation - sequential monte carlo, in J. Feret and H. Koepll, eds, ‘Computational Methods in Systems Biology’, Vol. 10545, Springer International Publishing, pp. 128–144. Series Title: Lecture Notes in Computer Science.
- [29] Klinger, E., Rickert, D. and Hasenauer, J. 2018, ‘pyabc: distributed, likelihood-free inference’, *Bioinformatics* (May), 1–3.
- [30] Kohn, L. M. and Anderson, J. B. 2014, ‘The underlying structure of adaptation under strong selection in 12 experimental yeast populations’, *Eukaryot. Cell* **13**(9), 1200–1206.

- [31] Komarova, N. L., Sengupta, A. and Nowak, M. A. 2003, ‘Mutation-selection networks of cancer initiation: Tumor suppressor genes and chromosomal instability’, *Journal of Theoretical Biology* **223**(4), 433–450.
- [32] Kumaran, R., Yang, S.-Y. and Leu, J.-Y. 2013, ‘Characterization of chromosome stability in diploid, polyploid and hybrid yeast cells’, *PLoS ONE* **8**(7), e68094.
- [33] Lauer, S., Avecilla, G., Spealman, P., Sethia, G., Brandt, N., Levy, S. F. and Gresham, D. 2018, ‘Single-cell copy number variant detection reveals the dynamics and diversity of adaptation.’, *PLOS Biology* **16**.
- [34] Lukow, D. A., Sausville, E. L., Suri, P., Chunduri, N. K., Wieland, A., Leu, J., Smith, J. C., Girish, V., Kumar, A. A., Kendall, J., Wang, Z., Storchova, Z. and Sheltzer, J. M. 2021, ‘Chromosomal instability accelerates the evolution of resistance to anti-cancer therapies’, *Developmental Cell* **56**(17), 2427–2439.e4.
- [35] Lynch, M., Sung, W., Morris, K., Coffey, N., Landry, C. R., Dopman, E. B., Dickinson, W. J., Okamoto, K., Kulkarni, S., Hartl, D. L. and Thomas, W. K. 2008, ‘A genome-wide view of the spectrum of spontaneous mutations in yeast’, *Proceedings of the National Academy of Sciences* **105**(27), 9272–9277.
- [36] Mannaert, A., Downing, T., Imamura, H. and Dujardin, J. C. 2012, ‘Adaptive mechanisms in pathogens: Universal aneuploidy in *Leishmania*’, *Trends Parasitol.* **28**(9), 370–376.
- [37] Möller, M., Habig, M., Freitag, M. and Stukenbrock, E. H. 2018, ‘Extraordinary genome instability and widespread chromosome rearrangements during vegetative growth’, *Genetics* **210**(2), 517–529.
- [38] Naylor, R. M. and van Deursen, J. M. 2016, ‘Aneuploidy in cancer and aging’, *Annu. Rev. Genet.* **50**(1), 45–66.
- [39] Niwa, O., Tange, Y. and Kurabayashi, A. 2006, ‘Growth arrest and chromosome instability in aneuploid yeast’, *Yeast* **23**(13), 937–950.
- [40] Otto, S. P. and Day, T. 2007, *A biologist’s guide to mathematical modeling in ecology and evolution*, Princeton University Press.
- [41] Pavelka, N., Rancati, G., Zhu, J., Bradford, W. D., Saraf, A., Florens, L., Sanderson, B. W., Hattem, G. L. and Li, R. 2010, ‘Aneuploidy confers quantitative proteome changes and phenotypic variation in budding yeast.’, *Nature* **468**(7321), 321–5.

- [42] Peter, J., De Chiara, M., Friedrich, A., Yue, J. X., Pflieger, D., Bergström, A., Sigwalt, A., Barre, B., Freel, K., Llored, A., Cruaud, C., Labadie, K., Aury, J. M., Istance, B., Lebrigand, K., Barbry, P., Engelen, S., Lemainque, A., Wincker, P., Liti, G. and Schacherer, J. 2018, ‘Genome evolution across 1,011 *Saccharomyces cerevisiae* isolates’, *Nature* **556**(7701), 339–344.
- [43] Ram, Y., Dellus-Gur, E., Bibi, M., Karkare, K., Obolski, U., Feldman, M. W., Cooper, T. F., Berman, J. and Hadany, L. 2019, ‘Predicting microbial growth in a mixed culture from growth curve data’, *Proceedings of the National Academy of Sciences* **116**(29), 14698–14707.
- [44] Rancati, G., Pavelka, N., Fleharty, B., Noll, A., Trimble, R., Walton, K., Perera, A., Staehling-Hampton, K., Seidel, C. W. and Li, R. 2008, ‘Aneuploidy underlies rapid adaptive evolution of yeast cells deprived of a conserved cytokinesis motor’, *Cell* **135**(5), 879–893.
- [45] Robbins, N., Caplan, T. and Cowen, L. E. 2017, ‘Molecular evolution of antifungal drug resistance’, *Annu. Rev. Microbiol.* **71**(1), 753–775.
- [46] Robinson, D., Vanacloig-Pedros, E., Cai, R., Place, M., Hose, J. and Gasch, A. P. 2023, ‘Gene-by-environment interactions influence the fitness cost of gene copy-number variation in yeast’, *bioRxiv*.
- [47] Rodrigues, M. L. and Albuquerque, P. C. 2018, ‘Searching for a change: The need for increased support for public health and research on fungal diseases’, *PLoS Negl. Trop. Dis.* **12**(6), 1–5.
- [48] Rutledge, S. D., Douglas, T. A., Nicholson, J. M., Vila-Casadesús, M., Kantzler, C. L., Wangsa, D., Barroso-Vilares, M., Kale, S. D., Logarinho, E. and Cimini, D. 2016, ‘Selective advantage of trisomic human cells cultured in non-standard conditions’, *Scientific Reports* **6**(June 2015), 1–12.
- [49] Santaguida, S. and Amon, A. 2015, ‘Short- and long-term effects of chromosome mis-segregation and aneuploidy’, *Nat. Rev. Mol. Cell Biol.* **16**(8), 473–485.
- [50] Santaguida, S., Vasile, E., White, E. and Amon, A. 2015, ‘Aneuploidy-induced cellular stresses limit autophagic degradation’, *Genes Dev.* **29**(19), 2010–2021.
- [51] Schwartzman, J. M., Sotillo, R. and Benezra, R. 2010, ‘Mitotic chromosomal instability and cancer: Mouse modelling of the human disease’, *Nat. Rev. Cancer* **10**(2), 102–115.
- [52] Selmecki, A. M., Dulmage, K., Cowen, L. E., Anderson, J. B. and Berman, J. 2009, ‘Acquisition of aneuploidy provides increased fitness during the evolution of antifungal drug resistance’, *PLoS Genet.* **5**(10), e1000705.

- 546 [53] Selmecki, A. M., Forche, A. and Berman, J. 2010, ‘Genomic plasticity of the human fungal  
pathogen *Candida albicans*’, *Eukaryot. Cell* **9**(7), 991–1008.
- 548 [54] Selmecki, A. M., Gerami-Nejad, M., Paulson, C., Forche, A. and Berman, J. 2008, ‘An isochro-  
mosome confers drug resistance in vivo by amplification of two genes, erg11 and tac1’, *Mol.  
Microbiol.* **68**(3), 624–641.
- 550 [55] Sheltzer, J. M. and Amon, A. 2011, ‘The aneuploidy paradox: Costs and benefits of an incorrect  
karyotype’, *Trends Genet.* **27**(11), 446–453.
- 552 [56] Sheltzer, J. M., Blank, H. M., Pfau, S. J., Tange, Y., George, B. M., Humpton, T. J., Brito, I. L.,  
554 Hiraoka, Y., Niwa, O. and Amon, A. 2011, ‘Aneuploidy drives genomic instability in yeast’,  
*Science* **333**(6045), 1026–1030.
- 556 [57] Sheltzer, J. M., Ko, J. H., Replogle, J. M., Habibe Burgos, N. C., Chung, E. S., Meehl, C. M.,  
Sayles, N. M., Passerini, V., Storchova, Z. and Amon, A. 2017, ‘Single-chromosome gains  
558 commonly function as tumor suppressors’, *Cancer Cell* **31**(2), 240–255.
- 559 [58] Sionov, E., Lee, H., Chang, Y. C. and Kwon-Chung, K. J. 2010, ‘*Cryptococcus neoformans*  
560 overcomes stress of azole drugs by formation of disomy in specific multiple chromosomes’,  
*PLoS Pathog.* **6**(4), e1000848.
- 562 [59] Sisson, S. A., Fan, Y. and Tanaka, M. M. 2007, ‘Sequential monte carlo without likelihoods’,  
*Proceedings of the National Academy of Sciences* **104**(6), 1760–1765.
- 564 [60] Sonti, R. V. and Roth, J. R. 1989, ‘Role of gene duplications in the adaptation of *Salmonella  
typhimurium* to growth on limiting carbon sources.’, *Genetics* **123**(1), 19–28.
- 566 [61] Syga, S., David-Rus, D., Schälte, Y., Hatzikirou, H. and Deutsch, A. 2021, ‘Inferring the effect  
of interventions on covid-19 transmission networks’, *Scientific Reports* **11**(1), 1–11.
- 568 [62] Todd, R. T., Forche, A. and Selmecki, A. M. 2017, ‘Ploidy variation in fungi: Polyploidy,  
aneuploidy, and genome evolution’, *Microbiol. Spectr.* **5**(4), 1–20.
- 570 [63] Toni, T., Welch, D., Strelkowa, N., Ipsen, A. and Stumpf, M. P. 2009, ‘Approximate bayesian  
computation scheme for parameter inference and model selection in dynamical systems’, *J. R.  
Soc. Interface* **6**(31), 187–202.
- 572 [64] Torres, E. M., Dephoure, N., Panneerselvam, A., Tucker, C. M., Whittaker, C. A., Gygi, S. P.,  
Dunham, M. J. and Amon, A. 2010, ‘Identification of aneuploidy-tolerating mutations’, *Cell*  
**143**(1), 71–83.

- 576 [65] Torres, E. M., Sokolsky, T., Tucker, C. M., Chan, L. Y., Boselli, M., Dunham, M. J. and Amon, A. 2007, ‘Effects of aneuploidy on cellular physiology and cell division in haploid yeast’, *Science* (80-. ). **317**(5840), 916–924.
- 578
- 580 [66] Tsai, H. J., Nelliat, A. R., Choudhury, M. I., Kucharavy, A., Bradford, W. D., Cook, M. E., Kim, J., Mair, D. B., Sun, S. X., Schatz, M. C. and Li, R. 2019, ‘Hypo-osmotic-like stress underlies general cellular defects of aneuploidy’, *Nature* .
- 582 [67] Williams, B. R., Prabhu, V. R., Hunter, K. E., Glazier, C. M., Whittaker, C. a., Housman, D. E. and Amon, A. 2008, ‘Aneuploidy affects proliferation and spontaneous immortalization in mammalian cells’, *Science* **322**(5902), 703–709.
- 584
- 586 [68] Yang, F., Todd, R. T., Selmecki, A., Jiang, Y. Y., Cao, Y. B. and Berman, J. 2021, ‘The fitness costs and benefits of trisomy of each *Candida albicans* chromosome’, *Genetics* **218**(2), 1–7.
- 588 [69] Yona, A. H., Frumkin, I. and Pilpel, Y. 2015, ‘A relay race on the evolutionary adaptation spectrum’, *Cell* **163**(3), 549–559.
- 590 [70] Yona, A. H., Manor, Y. S., Herbst, R. H., Romano, G. H., Mitchell, A., Kupiec, M., Pilpel, Y. and Dahan, O. 2012, ‘Chromosomal duplication is a transient evolutionary solution to stress.’, *Proceedings of the National Academy of Sciences* **109**(51), 21010–5.
- 592 [71] Zhu, J., Pavelka, N., Bradford, W. D., Rancati, G. and Li, R. 2012, ‘Karyotypic determinants of chromosome instability in aneuploid budding yeast’, *PLoS Genetics* **8**(5).
- 594 [72] Zhu, J., Tsai, H.-J., Gordon, M. R. and Li, R. 2018, ‘Cellular stress associated with aneuploidy’, *Dev. Cell* **44**(4), 420–431.
- 596 [73] Zhu, Y. O., Sherlock, G. and Petrov, D. A. 2016, ‘Whole genome analysis of 132 clinical *Saccharomyces cerevisiae* strains reveals extensive ploidy variation’, *G3 Genes, Genomes, Genetics* **6**(8), 2421–2434.
- 600 [74] Zhu, Y. O., Siegal, M. L., Hall, D. W. and Petrov, D. A. 2014, ‘Precise estimates of mutation rate and spectrum in yeast’, *Proceedings of the National Academy of Sciences* **111**(22), E2310–E2318.

# Supplementary Material

## 602 Supplementary Analysis

604 **Sensitivity analysis.** Changing a single parameter while keeping the rest fixed at the MAP estimate  
604 produces a worse fit to the data (Figure S6). Furthermore, we fitted models with a mutation rate  
fixed at  $\mu = 10^{-5}$ ,  $10^{-6}$  and  $10^{-7}$ . We inferred similar parameters estimates for the model with  
606  $\mu = 10^{-6}$  compared to the model with a free  $\mu$  parameter, in which the inferred mutation rate is  
 $\mu \approx 3 \cdot 10^{-6}$ . Inference assuming  $\mu = 10^{-5}$  or  $\mu = 10^{-7}$  produced similar estimates except that the  
608 estimated aneuploidy rate,  $\delta$ , was higher, and assuming  $\mu = 10^{-7}$ , the estimated fitness of  $2n+1$  was  
lower (Figure S7).

610 **Extended informative prior distribution.** In an extended informative prior distribution, we used  
additional growth curves of  $2n^*$  (*refined* strain from Yona et al.<sup>70</sup>) and  $2n+1$  in 39 °C to estimate  
612  $w_{2n^*}/w_{2n+1}$  (Figure S3H). The same distribution was used for  $w_{2n^*}/w_{2n+1*}$ . Thus, our main infor-  
614 mative prior uses a single prior distribution for fitness values of  $2n+1$ ,  $2n+1^*$ , and  $2n^*$ , whereas the  
extended informative prior uses one distribution for  $2n+1$ , and another distribution for both  $2n+1^*$   
and  $2n^*$ .

616 We estimated the parameters under this extended informative prior. Inference took much longer  
to run but the posterior distribution seemed to converge, as it did not change much in the final  
618 iterations. The posterior predictive plot shows that inference with this extended prior produces a  
posterior distribution that fails to explain the empirical observations (pink in Figure 3). However,  
620 the inferred posterior distribution is considerably narrower (compare Figures 2 and S8) and therefore  
parameter estimates are less variable. The estimated mutation rate was much lower compared to  
622 the main informative prior, with  $\mu = 2.474 \cdot 10^{-9}$  [ $2.423 \cdot 10^{-9} - 2.612 \cdot 10^{-9}$ ]. Other parameter  
estimates are:  $\delta = 2.705 \cdot 10^{-3}$  [ $2.094 \cdot 10^{-3} - 3.094 \cdot 10^{-3}$ ],  $w_{2n+1} = 1.022$  [ $1.021 - 1.024$ ],  
624  $w_{2n+1*} = 1.052$  [ $1.05 - 1.054$ ],  $w_{2n^*} = 1.053$  [ $1.051 - 1.055$ ], the latter two being much higher  
compare to the main informative prior. Notably, the mode of the posterior ratio  $w_{2n^*}/w_{2n+1} = 1.0009$   
626 is much lower than the mode of the prior ratio of 1.033 (Figure S3H) and closer to the ratio of 1 that  
we assume in the main informative prior. Together with the posterior predictive results, we conclude  
628 that the main informative prior is preferable over the extended informative prior.

630 **Model with transitions to less-fit genotypes** We also estimated the parameters of a version of the  
model that includes transitions (mutation, chromosome loss and gain) to less-fit genotypes (e.g.,  $2n^*$

to  $2n+1^*$ ),

$$\begin{aligned}
 f_{2n}^m &= (1 - \delta - \mu)f_{2n}^s + \delta f_{2n+1}^s + \mu f_{2n^*}^s , \\
 f_{2n+1}^m &= \delta f_{2n}^s + (1 - \delta - \mu)f_{2n+1}^s + \mu f_{2n+1^*}^s , \\
 f_{2n+1^*}^m &= \mu f_{2n+1}^s + (1 - \delta - \mu)f_{2n+1^*}^s + \delta f_{2n^*}^s , \\
 f_{2n^*}^m &= \mu f_{2n}^s + \delta f_{2n+1^*}^s + (1 - \delta - \mu)f_{2n^*}^s .
 \end{aligned} \tag{7}$$

The inferred values are slightly different. The estimated mutation rate,  $\mu = 1.036 \cdot 10^{-7}$  [8.01 · 10<sup>-8</sup> – 1.339 · 10<sup>-7</sup>], corresponds to a mutation target size of  $\sim 300$  – 500, assuming the mutation rate per base pair is roughly  $2 \cdot 10^{-10}$  (ref.<sup>74</sup>) or  $3.3 \cdot 10^{-10}$  (ref.<sup>35</sup>). The estimated aneuploidy rate,  $\delta = 2.358 \cdot 10^{-4}$  [ $1.766 \cdot 10^{-4}$  –  $2.837 \cdot 10^{-4}$ ] is 5-35-fold higher than in previous studies: for Chromosome III in diploid *S. cerevisiae*, Zhu et al.<sup>74</sup> estimated  $6.7 \cdot 10^{-6}$  chromosome gain events per generation, and Kumaran et al.<sup>32</sup> estimate  $3.0$  –  $4.3 \cdot 10^{-5}$  chromosome loss events per generation (95% confidence interval). The estimated fitness values are  $w_{2n+1} = 1.024$  [1.023 – 1.025],  $w_{2n+1^*} = 1.025$  [1.024 – 1.026],  $w_{2n^*} = 1.032$  [1.031 – 1.033], all relative to the fitness of  $2n$ , which is set to  $w_{2n} = 1$ .

We simulated genotype frequency dynamics using parameter samples from the posterior distribution, and computed the posterior distribution of  $F_A$ . The mean  $F_A$  in this case is just 0.0189 [0.0004 – 0.1214 95% CI], lower than without the transitions to less-fit genotypes. Here,  $F_A$  is the sum of frequencies of both  $2n_A^*$  and  $2n + 1_A^*$ , which reaches a frequency of 0.0007. Out of 100,000 posterior samples, none had  $F_A$  above 0.05 (i.e., 5% of the population).

## Supplementary Figures & Tables

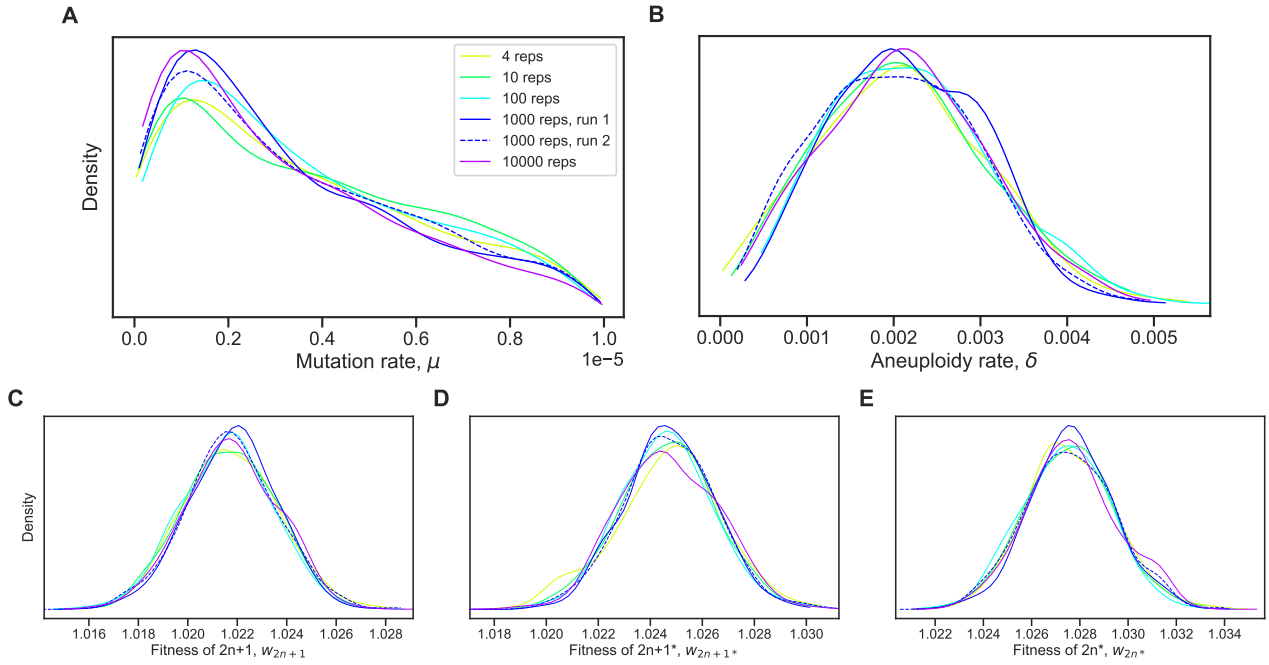


**Figure S1: Posterior distribution validation.** The posterior distribution of model parameters is roughly the same regardless of the number of simulations (4-10,000 replicates) used to approximate the likelihood (eq. (4)).

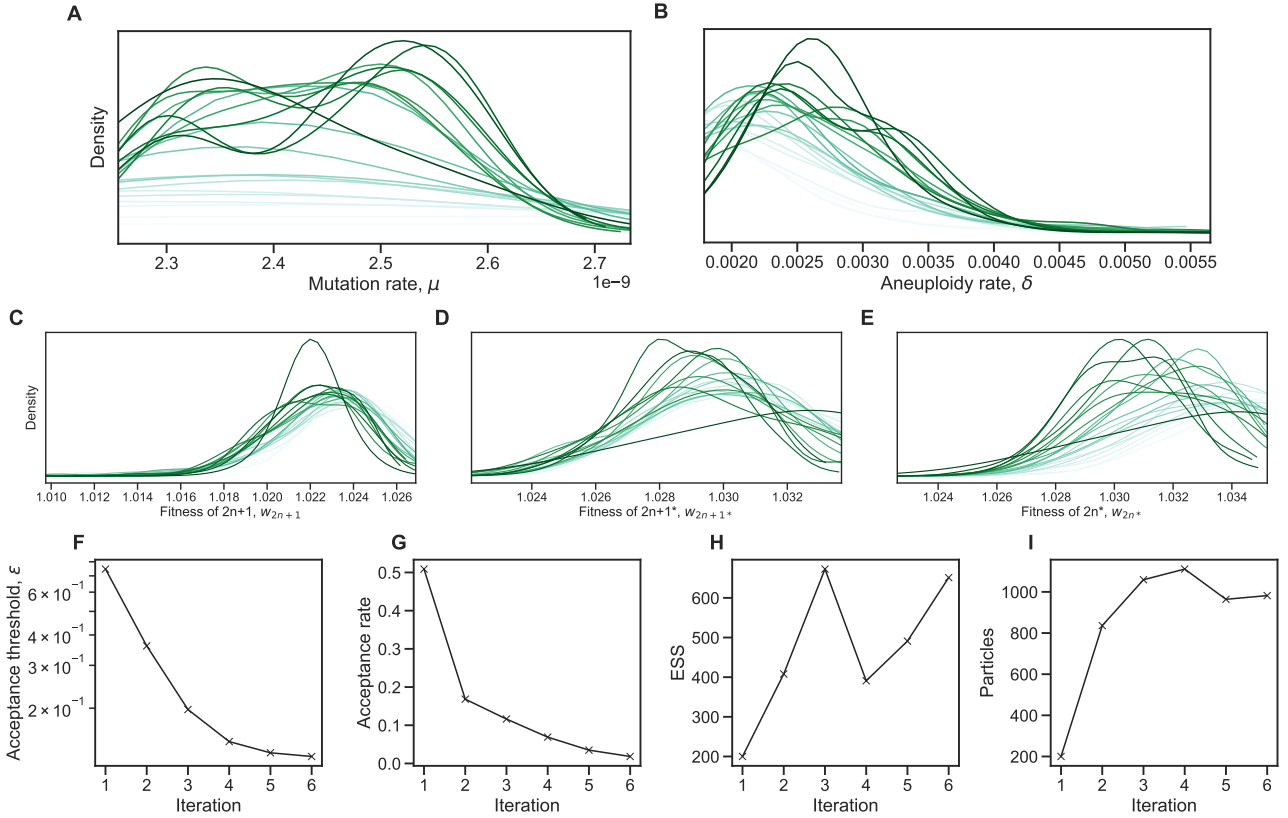


**Figure S2: Inference convergence.** The ABC-SMC algorithm was used to infer the model parameters. **(A-E)** The approximate posterior distributions of model parameters at each iteration of the ABC-SMC algorithm demonstrates convergence, as the posterior did not significantly change after the first iteration,  $t = 1$ . **(F-I)** ABC-SMC measures of convergence. After iteration number 6, the acceptance threshold was  $\epsilon = 0.13$  (i.e.,  $\mathcal{L} = 0.87$ , eq. (4)), the acceptance rate was 0.018, the number of particles was 982, and the effective sample size ESS=651.

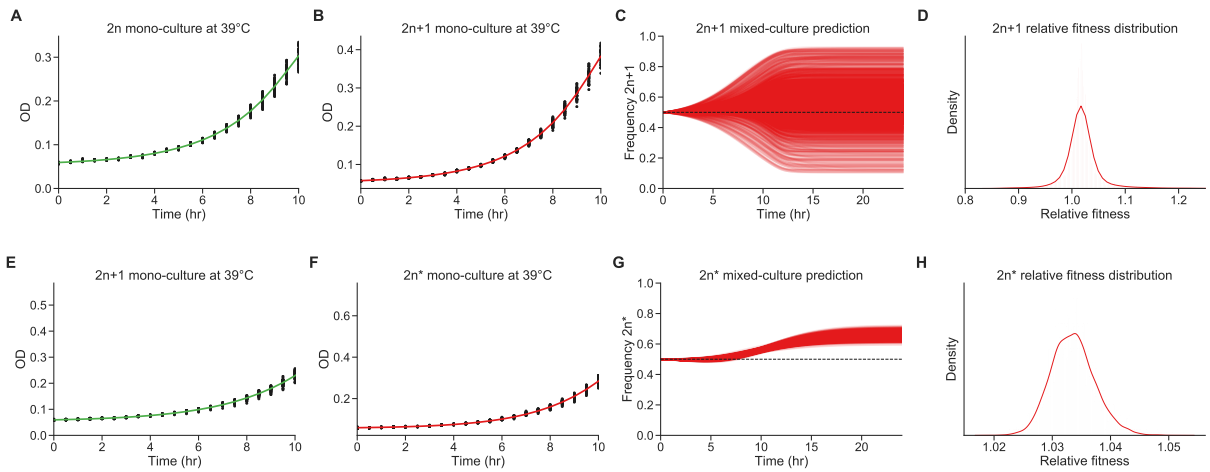


**Figure S3: Fitness estimation from growth curves.** **(A-D)** Fitness estimation from growth curves of  $2n$  and  $2n+1$  at  $39^{\circ}\text{C}$ .  $w_{2n+1}/w_{2n}=1.024$  (95% CI: 0.959 - 1.115). **Curveball (E-H)** Fitness estimation from growth curves of  $2n+1$  and  $2n^*$  at  $39^{\circ}\text{C}$ .  $w_{2n^*}/w_{2n+1}=1.033$  (95% CI: 1.027 - 1.041). Growth curves previously described in Yona et al.<sup>70</sup>, Figs. 3C, 4A, and S2. Fitness estimated from growth curves using Curveball, a method for predicting results of competition experiments from growth curve data<sup>43</sup> [curveball.yoavram.com](http://curveball.yoavram.com). See *Models and Methods, Prior distributions* for more details. **(A,B;E,F)** Mono-culture growth curve data (markers) and best-fit growth models (lines). **(C,G)** The mixed-culture prediction for the strains from A,B and E,F respectively, 6,375 generated curves. **(D,H)** The relative fitness distribution for  $2n+1$  relative to  $2n$  (panel D) and  $2n^*$  relative to  $2n+1$  (panel H). Figures generated by Curveball.

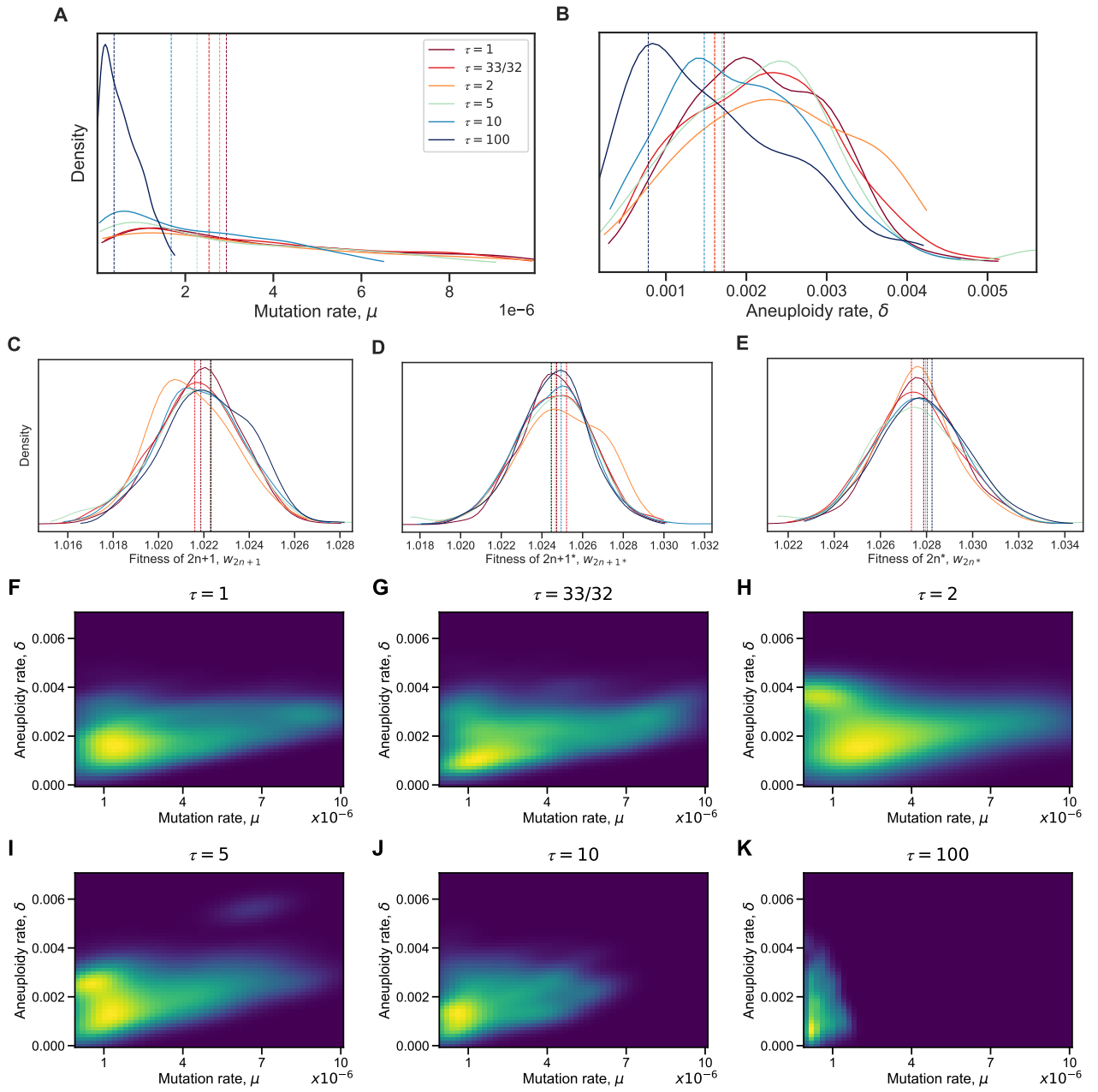


**Figure S4: Model with elevated mutation rate in aneuploid cells.** (A-E) The inferred posterior distributions for models with different values of  $\tau$ , the fold-increase in mutation rate in aneuploid cells ( $2n+1$  and  $2n+1^*$ ). Vertical dashed lines represent the MAP (maximum a posteriori) of each distribution. When the increase in mutation rate is high,  $\tau = 10$  and  $\tau = 100$ , the inferred mutation (A) and aneuploidy (B) rates tend to be lower. (F-K) The inferred joint posterior distribution of mutation rate ( $\mu$ ) and aneuploidy rate ( $\delta$ ) with different  $\tau$  values (dark purple and bright yellow for low and high density, respectively).

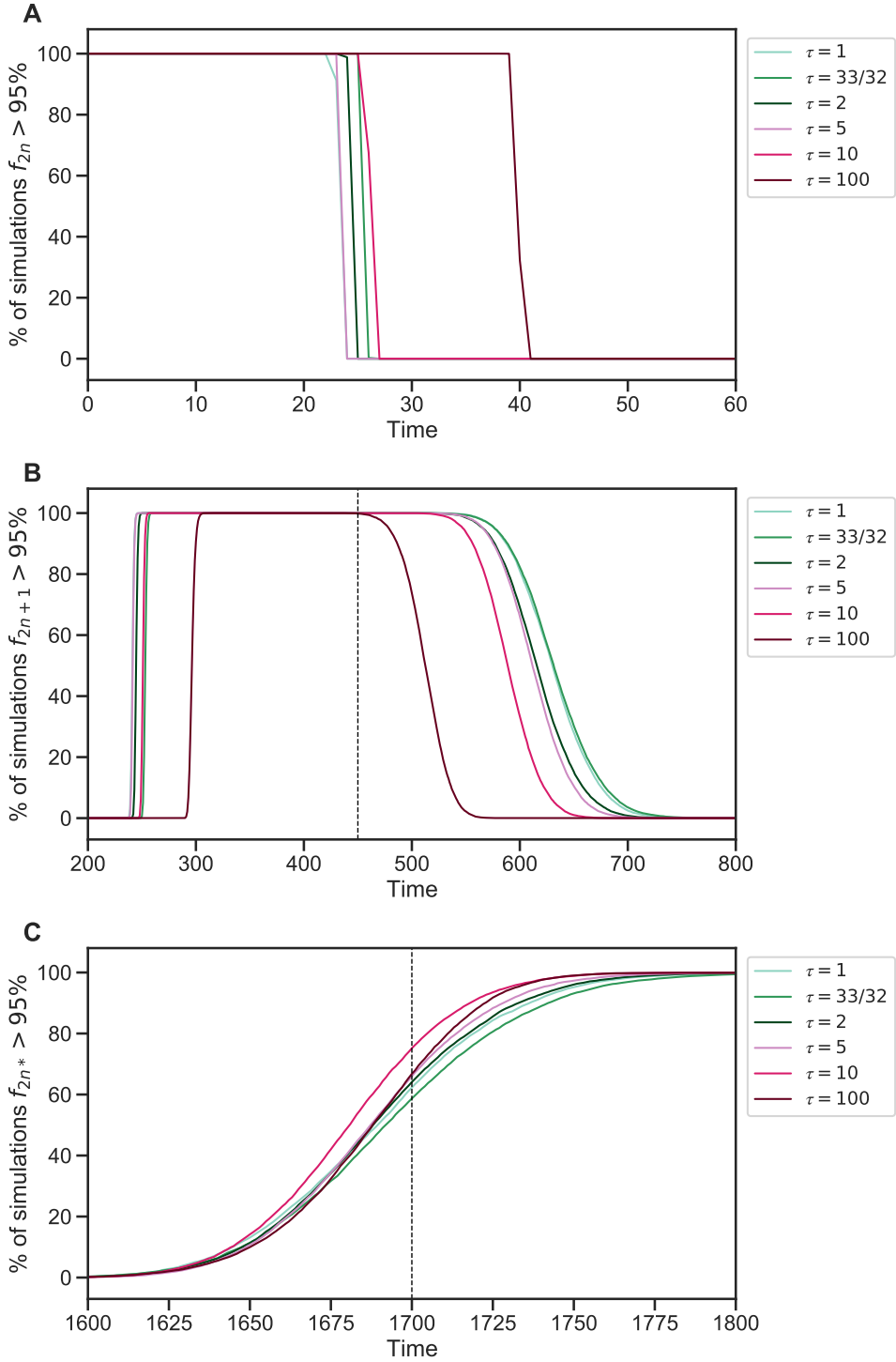


**Figure S5: Genotype fixations for models with increased genetic instability.** We estimated the parameters for different models, each assuming a different value of  $\tau$ , the fold-increase in mutation rate in aneuploid cells. We then generated 10,000 simulations using the MAP estimate of each model and evaluated the fraction of simulations in which the frequency of genotype  $2n$  (**A**),  $2n+1$  (**B**), and  $2n^*$  (**C**) is above 95% (y-axis) at each generation (x-axis). Note that  $2n+1^*$  did not fix. We can see that  $\tau = 100$  can be distinguished if the waiting time for  $f_{2n} < 95\%$  is known (panel A) or if the waiting time for  $f_{2n+1} > 95\%$  or  $f_{2n+1} < 95\%$  is known (panel B). It is harder to distinguish between  $1 \leq \tau \leq 10$ .

**Table S1: WAIC values for different  $\tau$  values.** Differences of less than 6 are considered of weak significance<sup>26</sup>.

Model	WAIC
$\tau = 1$	-9
$\tau = 33/32$	-9
$\tau = 2$	-8
$\tau = 5$	-12
$\tau = 10$	-9
$\tau = 100$	-12

WAIC defined in eq. (6).

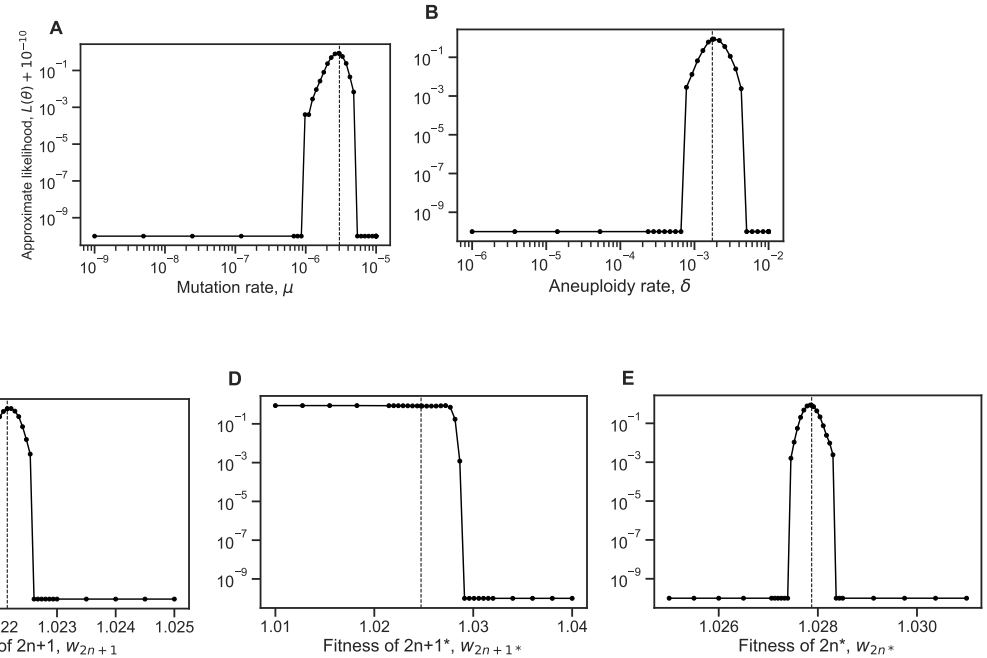


**Figure S6: Likelihood profiles.** Sensitivity of the model approximate likelihood,  $\mathcal{L}(\theta)$ , to changing a single parameter while the other parameters remain fixed at their MAP estimates. Dashed vertical line represents the MAP value. The prior distributions for the mutation rate and aneuploidy rate are  $\mu \sim U(10^{-9}, 10^{-5})$  and  $\delta \sim U(10^{-6}, 10^{-2})$ , respectively.

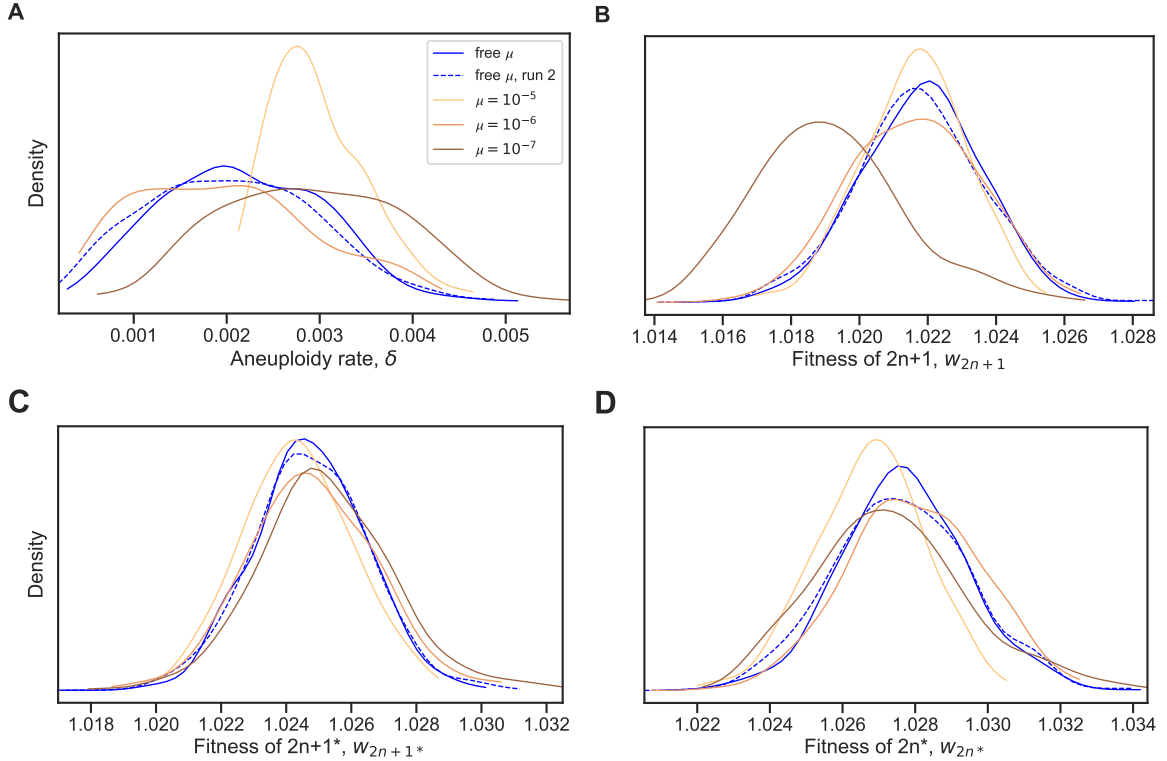


**Figure S7: Model with fixed mutation rate.** (A-D) The inferred posterior distributions for models with free and fixed mutation rate,  $\mu$ . The MAP (maximum a posteriori) and 50% HDI (highest density interval) for each model are: **free  $\mu$ , run 1:**  $\delta = 1.720 \cdot 10^{-3}$  [ $1.470 \cdot 10^{-3} - 2.786 \cdot 10^{-3}$ ],  $w_{2n+1} = 1.022$  [1.021 – 1.023],  $w_{2n+1^*} = 1.025$  [1.024 – 1.026],  $w_{2n^*} = 1.028$  [1.026 – 1.029]; **free  $\mu$ , run 2:**  $\delta = 2.129 \cdot 10^{-3}$  [ $1.334 \cdot 10^{-3} - 2.695 \cdot 10^{-3}$ ],  $w_{2n+1} = 1.022$  [1.02 – 1.023],  $w_{2n+1^*} = 1.025$  [1.023 – 1.026],  $w_{2n^*} = 1.028$  [1.026 – 1.029];  **$\mu = 10^{-5}$ :**  $\delta = 2.903 \cdot 10^{-3}$  [ $2.399 \cdot 10^{-3} - 3.156 \cdot 10^{-3}$ ],  $w_{2n+1} = 1.022$  [1.021 – 1.023],  $w_{2n+1^*} = 1.024$  [1.023 – 1.025],  $w_{2n^*} = 1.027$  [1.026 – 1.028];  **$\mu = 10^{-6}$ :**  $\delta = 1.917 \cdot 10^{-3}$  [ $9.624 \cdot 10^{-4} - 2.447 \cdot 10^{-3}$ ],  $w_{2n+1} = 1.022$  [1.02 – 1.023],  $w_{2n+1^*} = 1.025$  [1.023 – 1.026],  $w_{2n^*} = 1.028$  [1.027 – 1.029];  **$\mu = 10^{-7}$ :**  $\delta = 2.901 \cdot 10^{-3}$  [ $2.139 \cdot 10^{-3} - 3.671 \cdot 10^{-3}$ ],  $w_{2n+1} = 1.019$  [1.017 – 1.02],  $w_{2n+1^*} = 1.025$  [1.024 – 1.026],  $w_{2n^*} = 1.027$  [1.026 – 1.029].

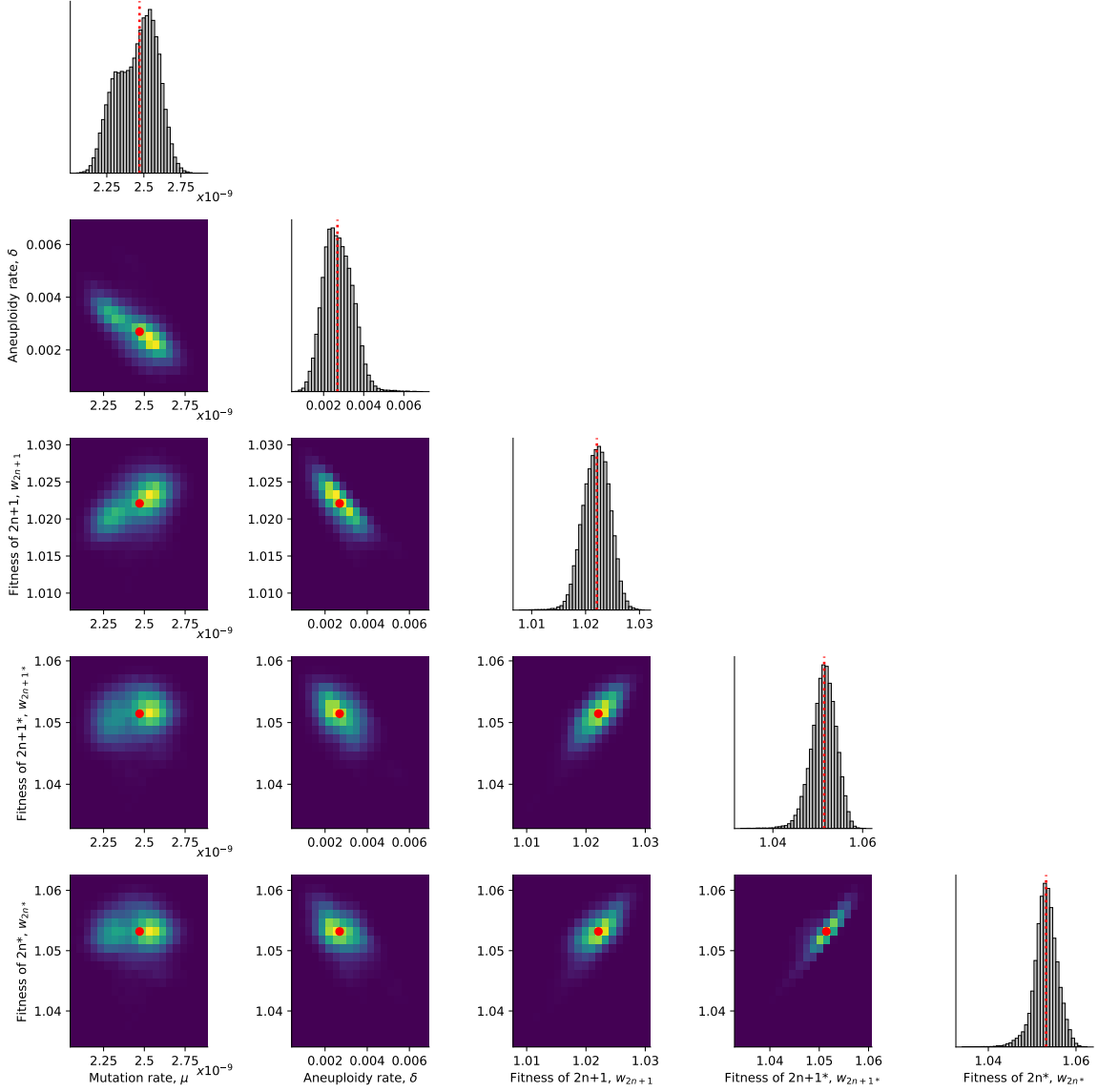


**Figure S8: Posterior distribution of parameters inferred with the extended prior distribution.** On the diagonal, the inferred posterior distribution of each model parameter. Below the diagonal, the inferred joint posterior distribution of pairs of model parameters (dark purple and bright yellow for low and high density, respectively). Red markers and orange lines for the joint MAP estimate (which may differ from the marginal MAP, as the marginal distribution integrates over all other parameters).

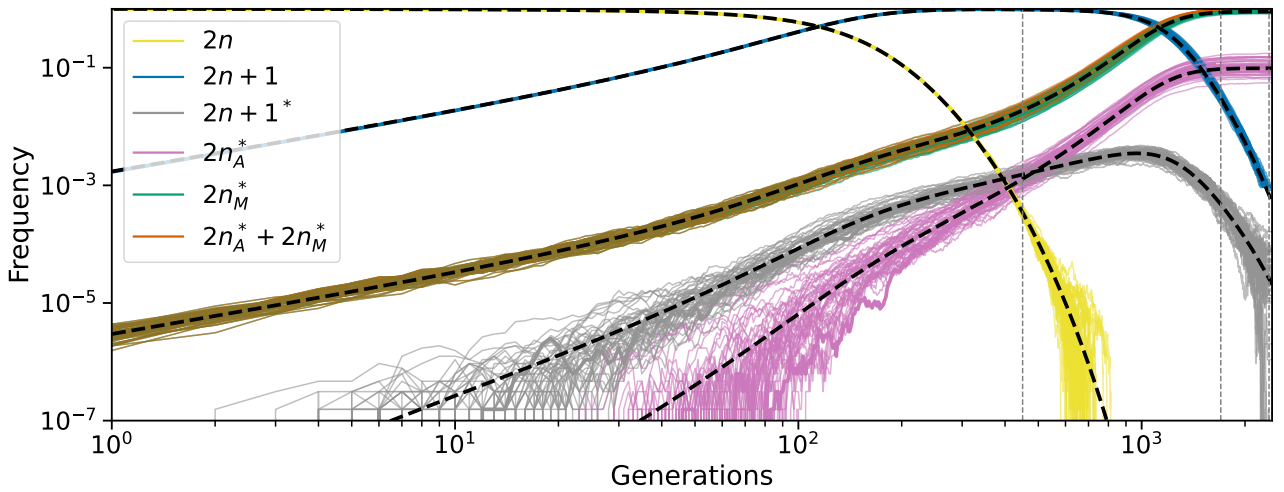


**Figure S9: Posterior predicted genotype frequencies in log-log scale.** Frequency dynamics of the different genotypes with MAP parameter estimates, same as Figure 4A, but in log-log scale. Black dashed curves for a deterministic model without genetic drift. Clearly, appearance of  $2n+1$  and  $2n_M^*$  is deterministic. Appearance of  $2n+1^*$ , and therefore  $2n_A^*$ , is stochastic, however, the frequency dynamics are deterministic above a frequency of roughly 0.001. Note that the  $2n_M^*$  and the  $2n_A^* + 2n_M^*$  lines are overlapping for much of their trajectories.

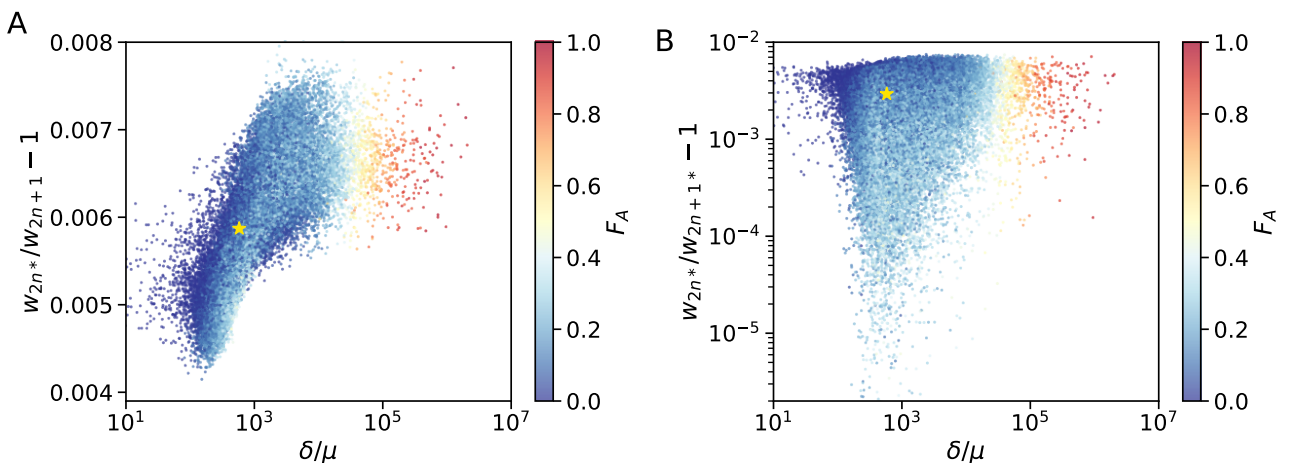


**Figure S10: Posterior distribution of  $F_A$ .** (A,B)  $F_A$  values (color coded) as in Figure 4 for different parameter choices on the x- and y-axes. White star denotes the MAP estimate.

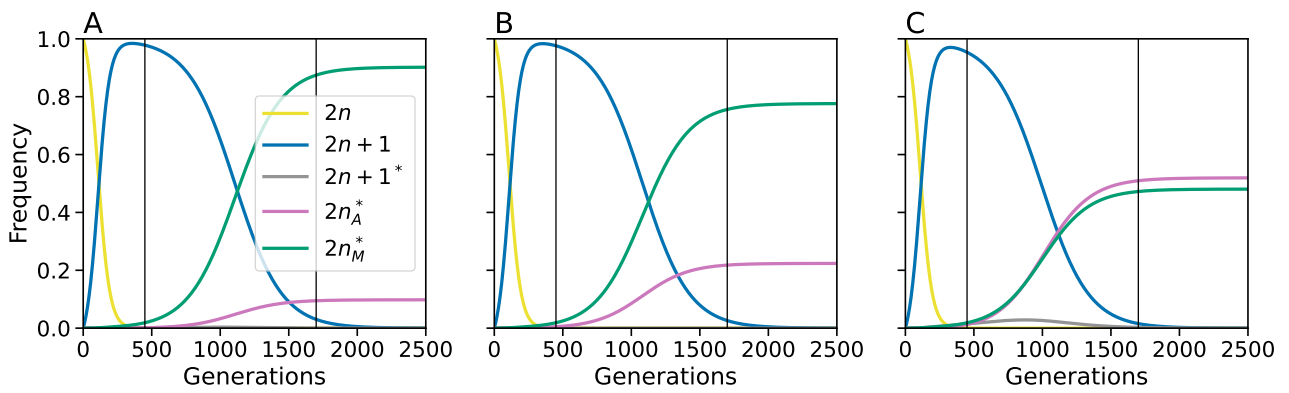


**Figure S11: Effect of genomic instability on genotype frequencies.** Genotype frequencies in the deterministic model without drift and with MAP parameter estimates (**A**), with 100-fold increase in rate of chromosome loss (transition from  $2n + 1^*$  to  $2n^*$ ) (**B**), and with 10-fold increase in mutation rate in aneuploid cells (**C**). Corresponding  $F_A$  values are 0.098, 0.223, and 0.519.